

Numerical methods of chaos detection

Haris Skokos

**Department of Mathematics and Applied Mathematics
University of Cape Town
Cape Town, South Africa**

**E-mail: haris.skokos@uct.ac.za – haris.skokos@gmail.com
URL: http://math_research.uct.ac.za/~hskokos/**

**Days of Applied Nonlinearity and Complexity (DANOC)
14 January 2024, Thessaloniki, Greece (online event)**

University of Cape Town (UCT)



University of Cape Town (UCT)



Cape Town



Outline

- **Dynamical Systems**
 - ✓ **Hamiltonian models – Variational equations**
 - ✓ **Symplectic maps – Tangent map**
- **Brief presentation of chaos detection methods**
- **Chaos Indicators**
 - ✓ **Lyapunov exponents**
 - ✓ **Smaller ALignment Index – SALI**
 - **Definition**
 - **Behavior for chaotic and regular motion**
 - **Applications**
 - ✓ **Generalized ALignment Index – GALI**
 - **Definition - Relation to SALI**
 - **Behavior for chaotic and regular motion**
 - **Application to time-dependent models**
- **Chaos diagnostics based on Lagrangian descriptors (LDs)**
- **Summary**

Autonomous Hamiltonian systems

Consider an **N degree of freedom** autonomous Hamiltonian system having a Hamiltonian function of the form:

$$H(\overbrace{q_1, q_2, \dots, q_N}^{\text{positions}}, \overbrace{p_1, p_2, \dots, p_N}^{\text{momenta}})$$

The time evolution of an orbit (trajectory) with initial condition

$$P(0) = (q_1(0), q_2(0), \dots, q_N(0), p_1(0), p_2(0), \dots, p_N(0))$$

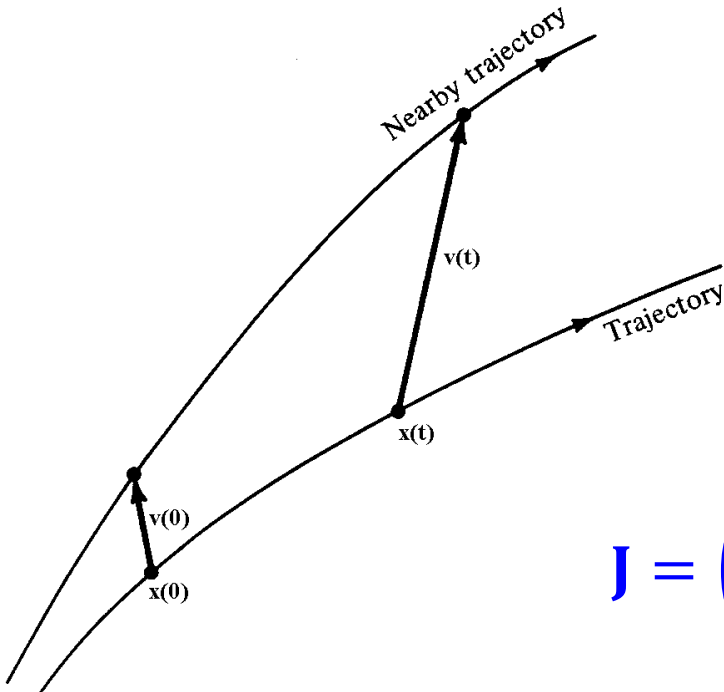
is governed by the **Hamilton's equations of motion**

$$\frac{dp_i}{dt} = -\frac{\partial H}{\partial q_i}, \quad \frac{dq_i}{dt} = \frac{\partial H}{\partial p_i}$$

Variational Equations

We use the notation $\mathbf{x} = (q_1, q_2, \dots, q_N, p_1, p_2, \dots, p_N)^T$. The **deviation vector** from a given orbit is denoted by

$$\mathbf{v} = (\delta x_1, \delta x_2, \dots, \delta x_n)^T, \text{ with } n=2N$$



The time evolution of \mathbf{v} is given by the so-called **variational equations**:

$$\frac{d\mathbf{v}}{dt} = -\mathbf{J} \cdot \mathbf{P} \cdot \mathbf{v}$$

where

$$\mathbf{J} = \begin{pmatrix} \mathbf{0}_N & -\mathbf{I}_N \\ \mathbf{I}_N & \mathbf{0}_N \end{pmatrix}, \mathbf{P}_{ij} = \frac{\partial^2 H}{\partial x_i \partial x_j} \quad i, j = 1, 2, \dots, n$$

Symplectic Maps

Consider an **2N-dimensional symplectic map T**. In this case we have **discrete time**.

The evolution of an **orbit** with initial condition

$$P(0) = (x_1(0), x_2(0), \dots, x_{2N}(0))$$

is governed by the **equations of map T**

$$P(i+1) = T P(i) \quad , \quad i = 0, 1, 2, \dots$$

The evolution of an initial **deviation vector**

$$v(0) = (\delta x_1(0), \delta x_2(0), \dots, \delta x_{2N}(0))$$

is given by the corresponding **tangent map**

$$v(i+1) = \left. \frac{\partial T}{\partial P} \right|_i \cdot v(i) \quad , \quad i = 0, 1, 2, \dots$$

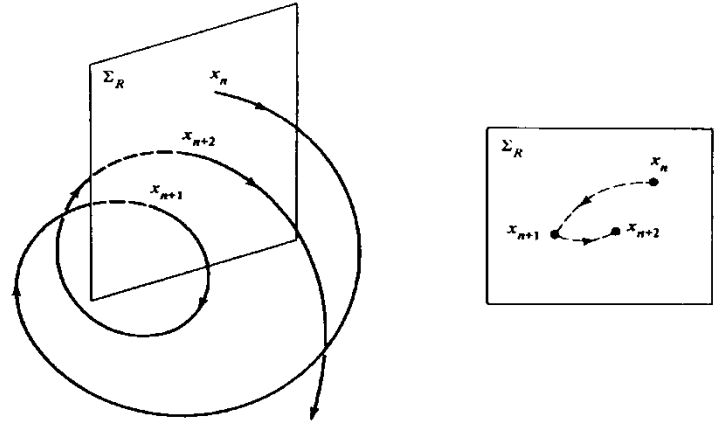
Chaos detection techniques

- **Based on the visualization of orbits**
 - ✓ **Poincaré Surface of Section (PSS)**
 - ✓ **the color and rotation (CR) method**
 - ✓ **the 3D phase space slices (3PSS) technique**

Poincaré Surface of Section (PSS)

We can constrain the study of an $N+1$ degree of freedom Hamiltonian system to a **2N-dimensional subspace of the general phase space**.

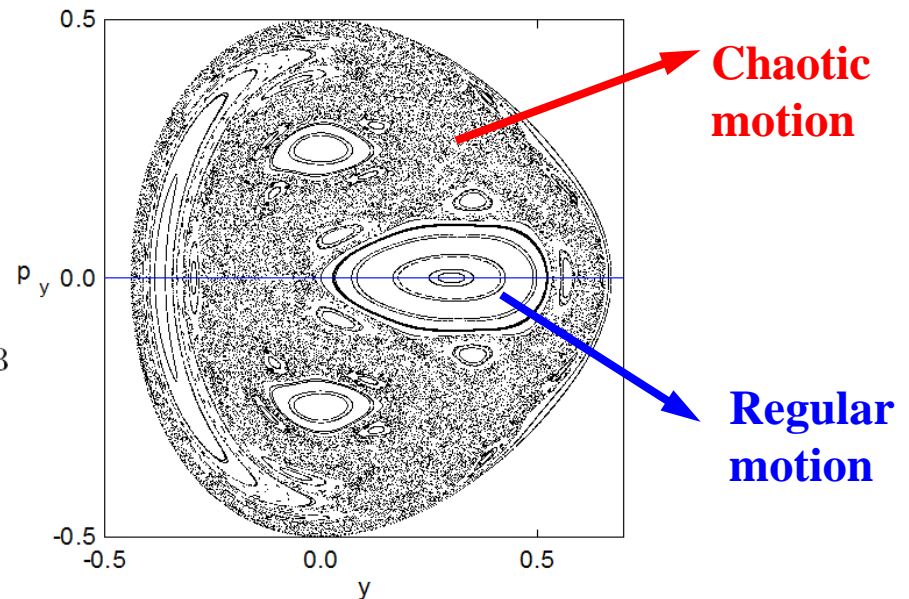
In this sense an $N+1$ degree of freedom Hamiltonian system corresponds to a **2N-dimensional symplectic map**.



Lieberman & Lichtenberg, 1992, *Regular and Chaotic Dynamics*, Springer.

The 2D Hénon-Heiles system:

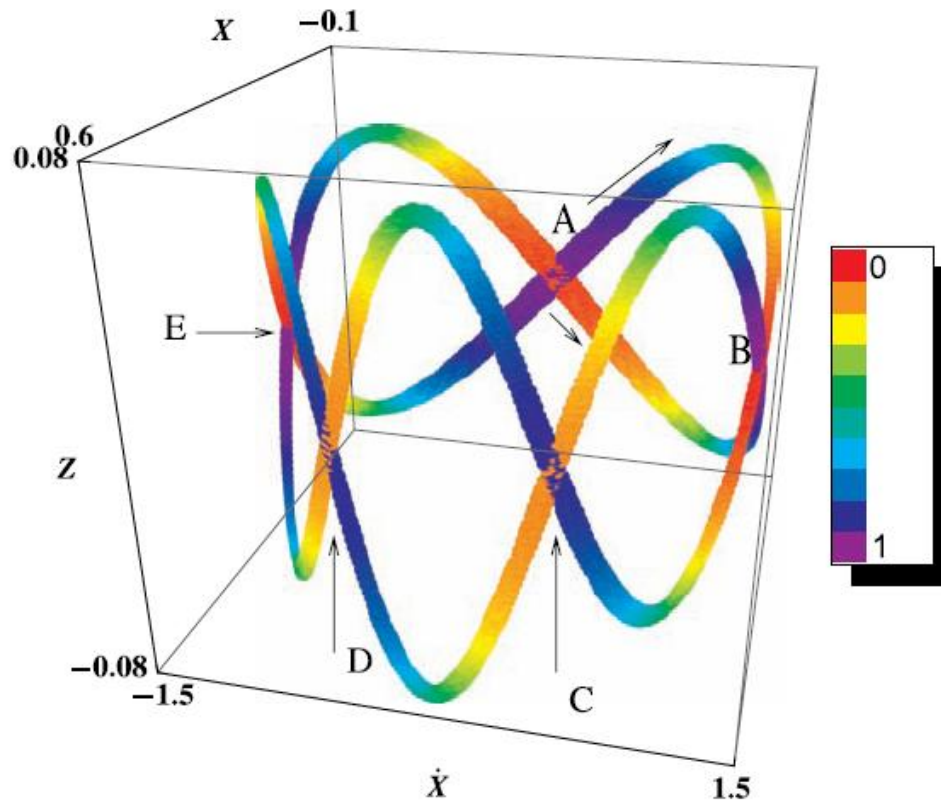
$$H_2 = \frac{1}{2}(p_x^2 + p_y^2) + \frac{1}{2}(x^2 + y^2) + x^2y - \frac{1}{3}y^3$$



The color and rotation (CR) method

For 3 degree of freedom Hamiltonian systems and 4 dimensional symplectic maps:

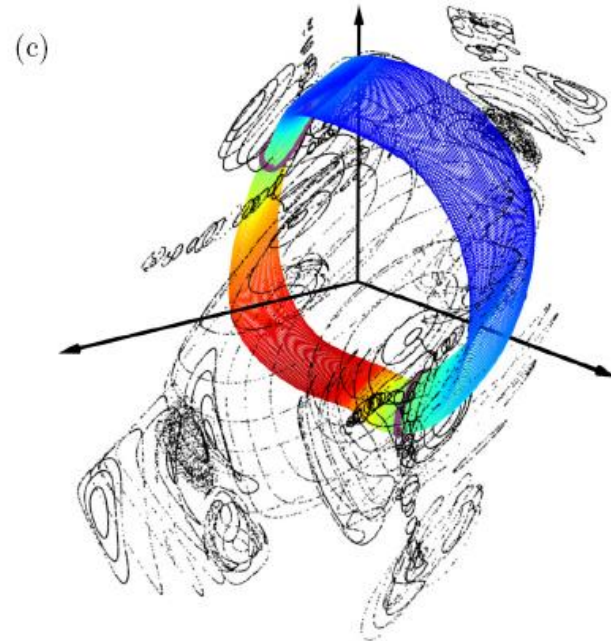
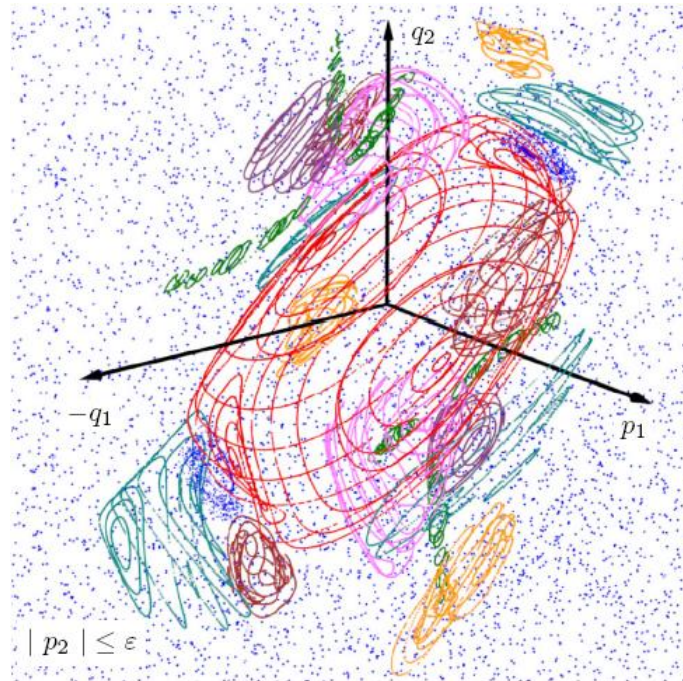
We consider the 3D projection of the PSS and use color to indicate the 4th dimension.



The 3D phase space slices (3PSS) technique

For 3 degree of freedom Hamiltonian systems and 4 dimensional symplectic maps:

We consider thin 3D phase space slices of the 4D phase space (e.g. $|p_2| \leq \epsilon$) and present intersections of orbits with these slices.

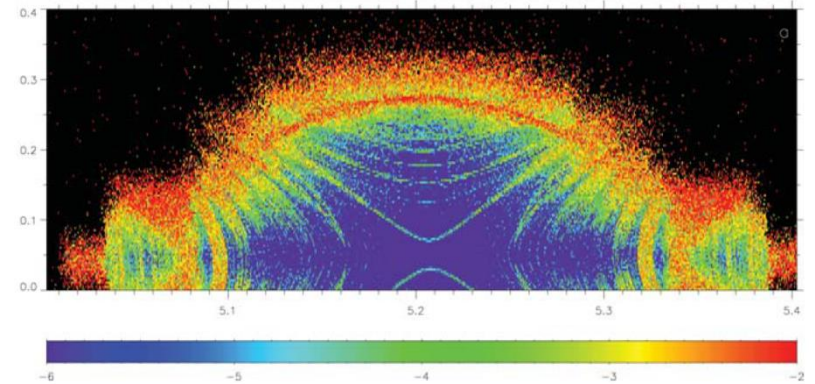


Chaos detection techniques

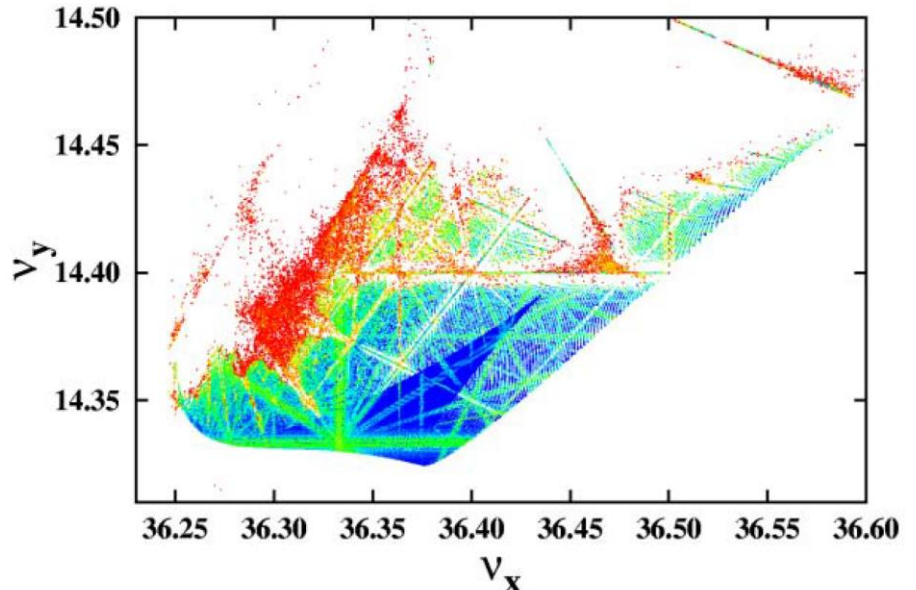
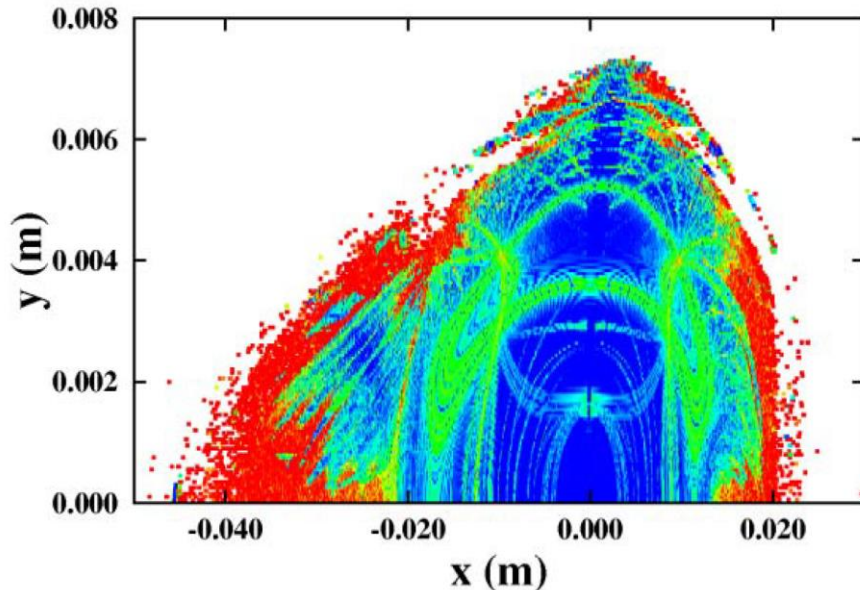
- **Based on the visualization of orbits**
 - ✓ **Poincaré Surface of Section (PSS)**
 - ✓ **the color and rotation (CR) method**
 - ✓ **the 3D phase space slices (3PSS) technique**
- **Based on the numerical analysis of orbits**
 - ✓ **Frequency Map Analysis**
 - ✓ **0-1 test**

Frequency Map Analysis

Stability of **Trojan asteroids**, (α, e) diagram [Robutel & Gabern, MNRAS (2006)]



Dynamics of **the European Synchrotron Radiation Facility (ESRF) storage ring** [S. et al., 2004, in Proc. of the 9th European Particle Accelerator Conf. (EPAC)]



Chaos detection techniques

- **Based on the visualization of orbits**
 - ✓ Poincaré Surface of Section (PSS)
 - ✓ the color and rotation (CR) method
 - ✓ the 3D phase space slices (3PSS) technique
- **Based on the numerical analysis of orbits**
 - ✓ Frequency Map Analysis
 - ✓ 0-1 test
- **Chaos indicators based on the evolution of deviation vectors from a given orbit**
 - ✓ Maximum Lyapunov Exponent (MLE)
 - ✓ Fast Lyapunov Indicator (FLI) and Orthogonal Fast Lyapunov Indicators (OFLI and OFLI2)
 - ✓ Mean Exponential Growth Factor of Nearby Orbits (MEGNO)
 - ✓ Relative Lyapunov Indicator (RLI)
 - ✓ **Smaller ALignment Index – SALI**
 - ✓ **Generalized ALignment Index – GALI**

Maximum Lyapunov Exponent (MLE)

Chaos: sensitive dependence on initial conditions.

Roughly speaking, the MLE of a given orbit characterizes the **mean exponential rate of divergence** of trajectories surrounding it.

Consider an orbit in the $2N$ -dimensional phase space with **initial condition $\mathbf{x}(0)$** and **an initial deviation vector (small perturbation) from it $\mathbf{v}(0)$** .

Then the mean exponential rate of divergence is:

$$\text{MLE} = \lambda_1 = \lim_{t \rightarrow \infty} \Lambda(t) = \lim_{t \rightarrow \infty} \frac{1}{t} \ln \frac{\|\mathbf{v}(t)\|}{\|\mathbf{v}(0)\|}$$

$\lambda_1 = 0 \rightarrow$ Regular motion ($\Lambda \propto t^{-1}$)

$\lambda_1 > 0 \rightarrow$ Chaotic motion

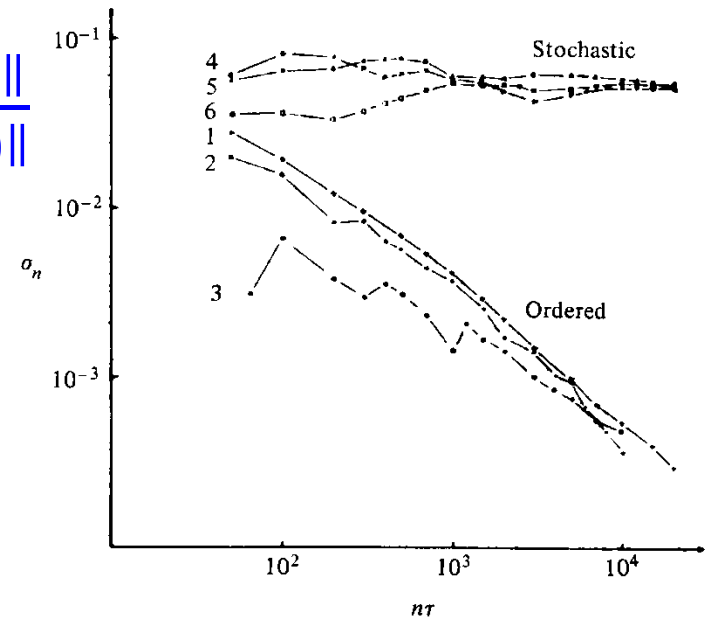


Figure 5.7. Behavior of σ_n at the intermediate energy $E = 0.125$ for initial points taken in the ordered (curves 1–3) or stochastic (curves 4–6) regions (after Benettin *et al.*, 1976).

**The
Smaller ALignment Index
(SALI)
method**

Definition of the SALI

We follow the evolution in time of two different initial deviation vectors ($\mathbf{v}_1(\mathbf{0})$, $\mathbf{v}_2(\mathbf{0})$), and define SALI [S., J. Phys. A (2001) – S. & Manos, Lect. Notes Phys. (2016)] as:

$$\text{SALI}(\mathbf{t}) = \min\{\|\hat{\mathbf{v}}_1(\mathbf{t}) + \hat{\mathbf{v}}_2(\mathbf{t})\|, \|\hat{\mathbf{v}}_1(\mathbf{t}) - \hat{\mathbf{v}}_2(\mathbf{t})\|\}$$

where

$$\hat{\mathbf{v}}_1(\mathbf{t}) = \frac{\mathbf{v}_1(\mathbf{t})}{\|\mathbf{v}_1(\mathbf{t})\|}$$

When the two vectors become collinear

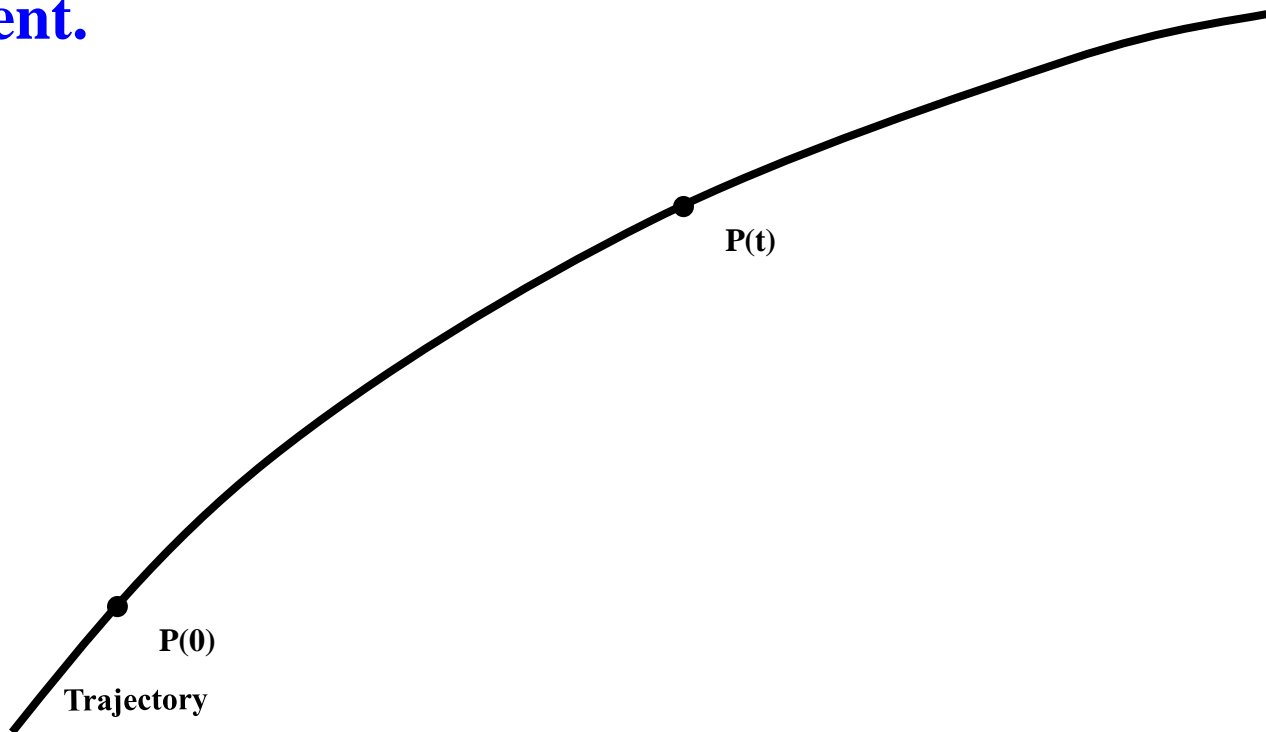
$$\text{SALI}(\mathbf{t}) \rightarrow 0$$

Behavior of SALI for **chaotic motion**

For chaotic orbits the two initially different deviation vectors tend to coincide with the direction defined by the maximum Lyapunov exponent.

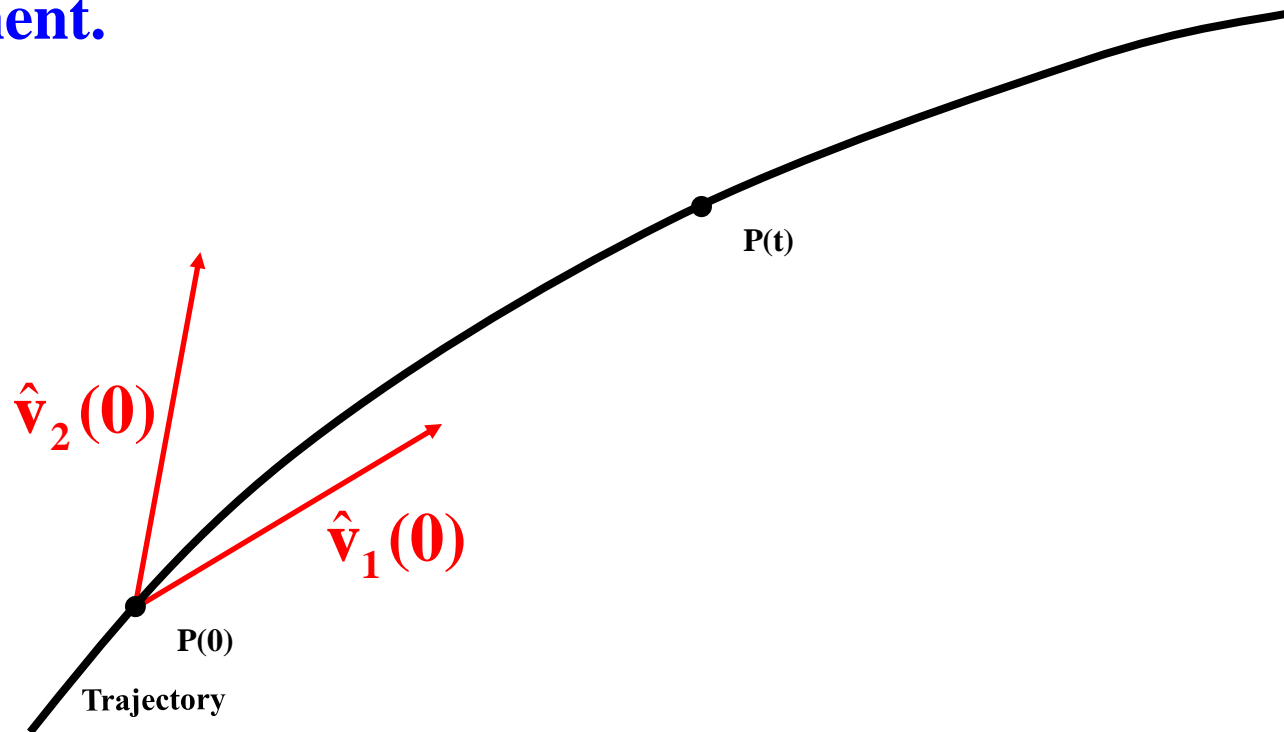
Behavior of SALI for **chaotic motion**

For chaotic orbits the two initially different deviation vectors tend to coincide with the direction defined by the maximum Lyapunov exponent.



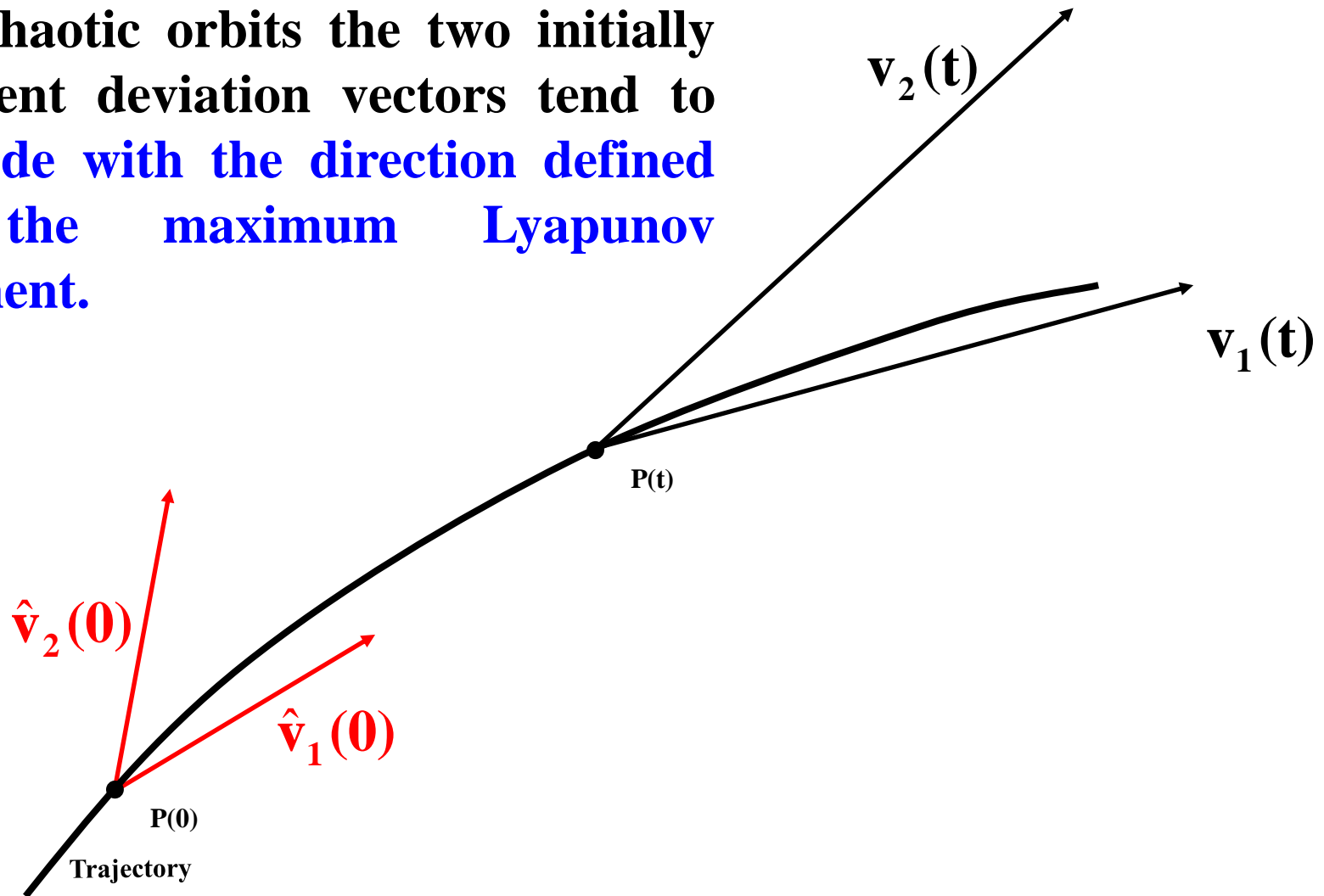
Behavior of SALI for **chaotic motion**

For chaotic orbits the two initially different deviation vectors tend to coincide with the direction defined by the maximum Lyapunov exponent.



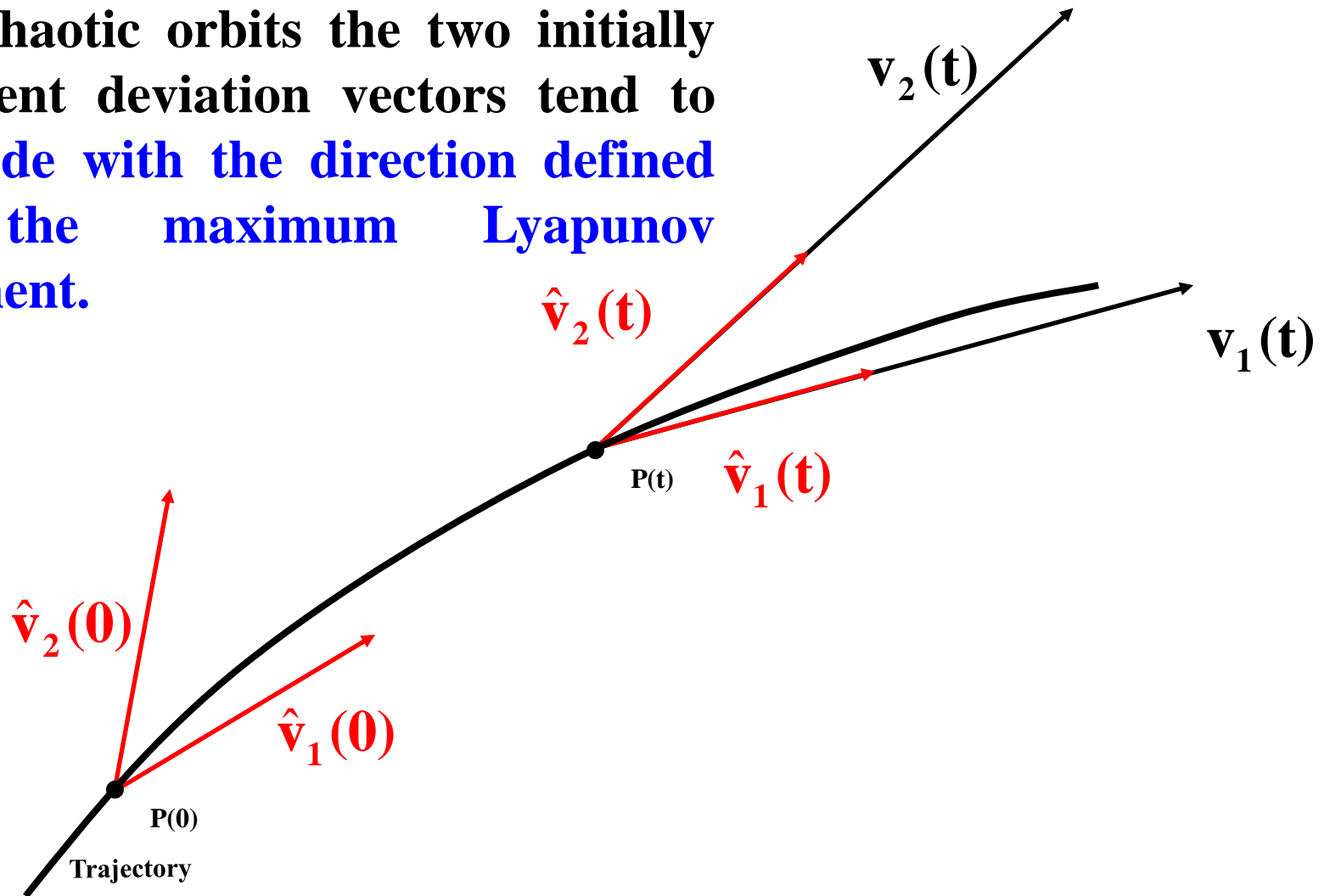
Behavior of SALI for **chaotic motion**

For chaotic orbits the two initially different deviation vectors tend to coincide with the direction defined by the maximum Lyapunov exponent.



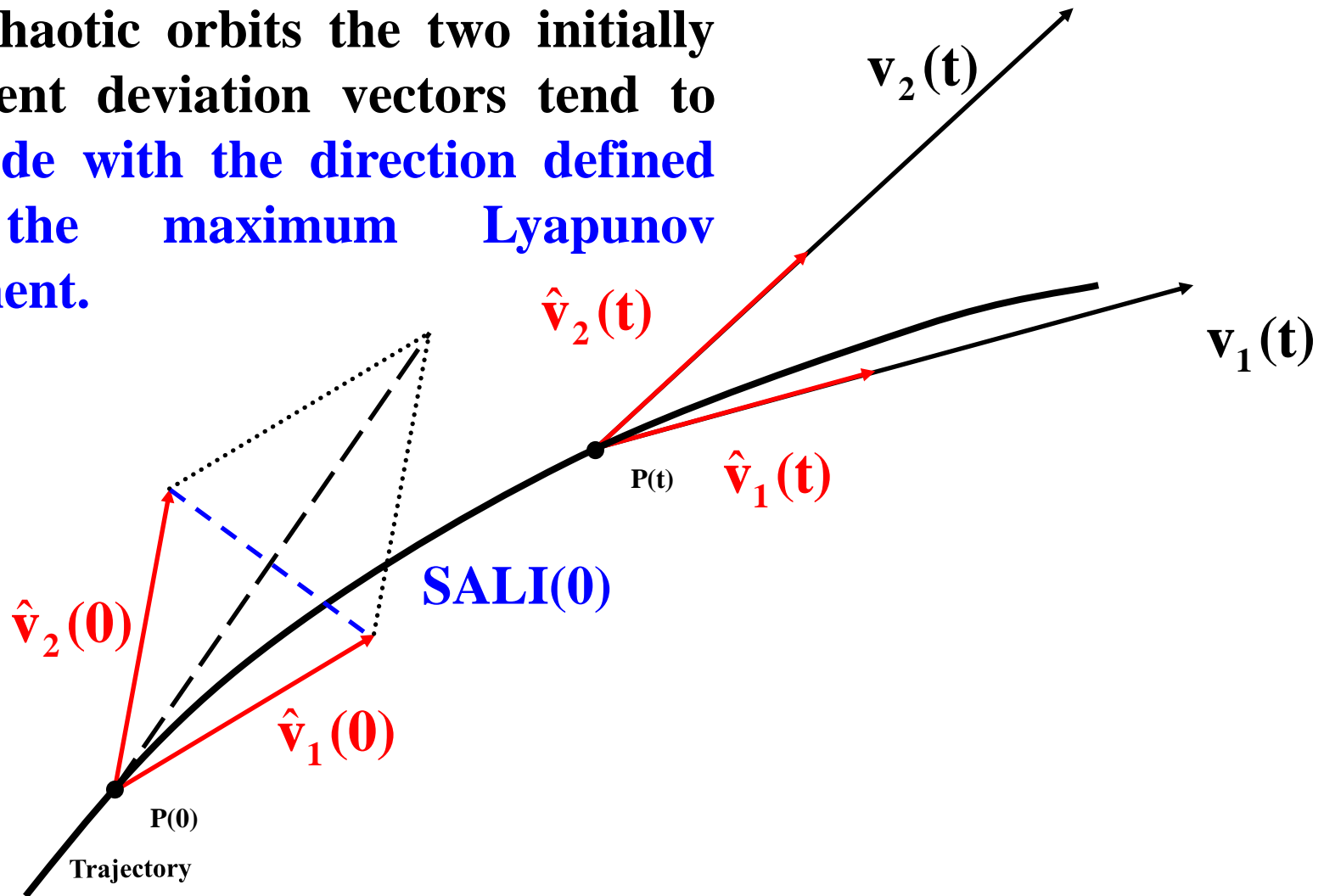
Behavior of SALI for **chaotic motion**

For chaotic orbits the two initially different deviation vectors tend to coincide with the direction defined by the maximum Lyapunov exponent.



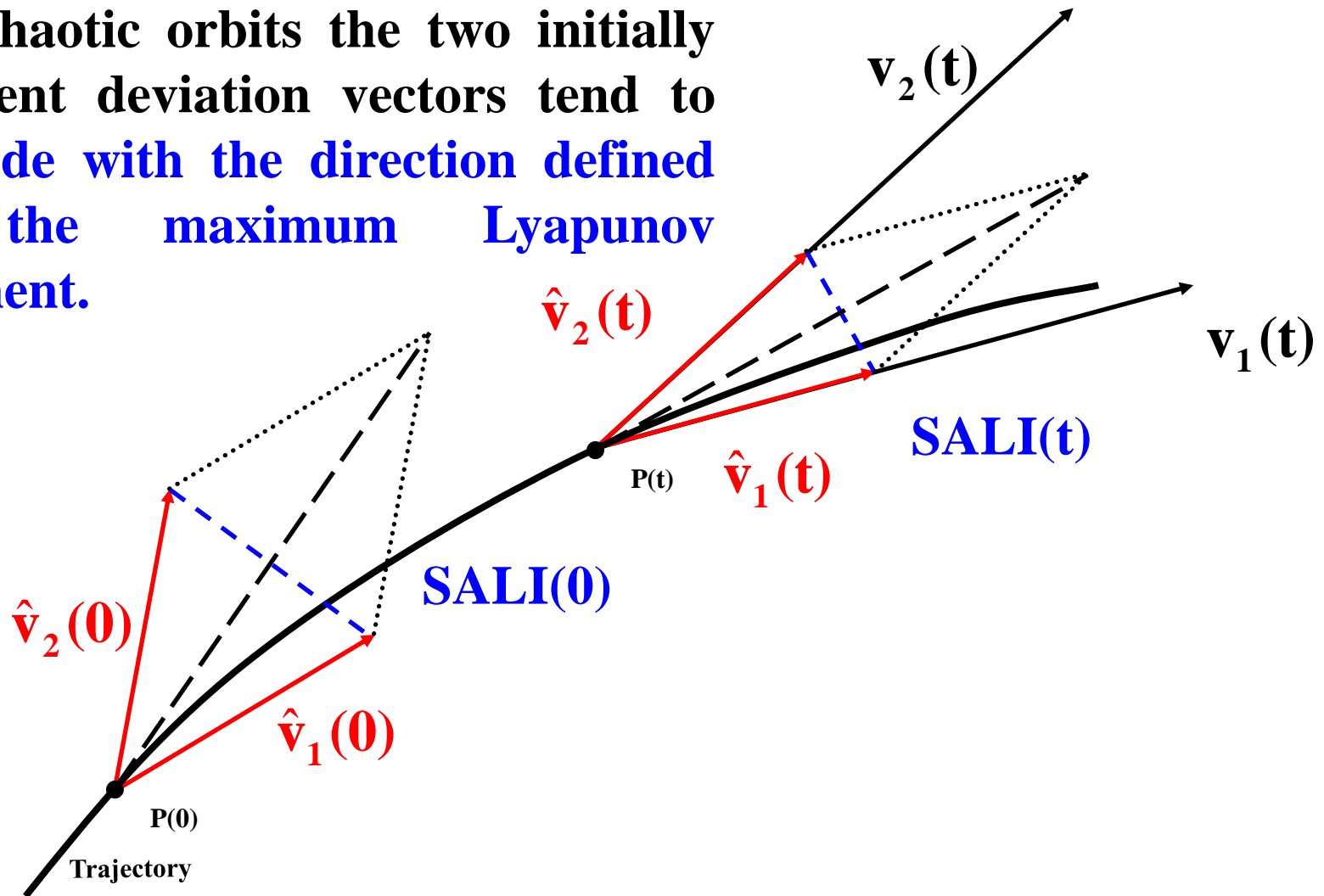
Behavior of SALI for chaotic motion

For chaotic orbits the two initially different deviation vectors tend to coincide with the direction defined by the maximum Lyapunov exponent.



Behavior of SALI for chaotic motion

For chaotic orbits the two initially different deviation vectors tend to coincide with the direction defined by the maximum Lyapunov exponent.

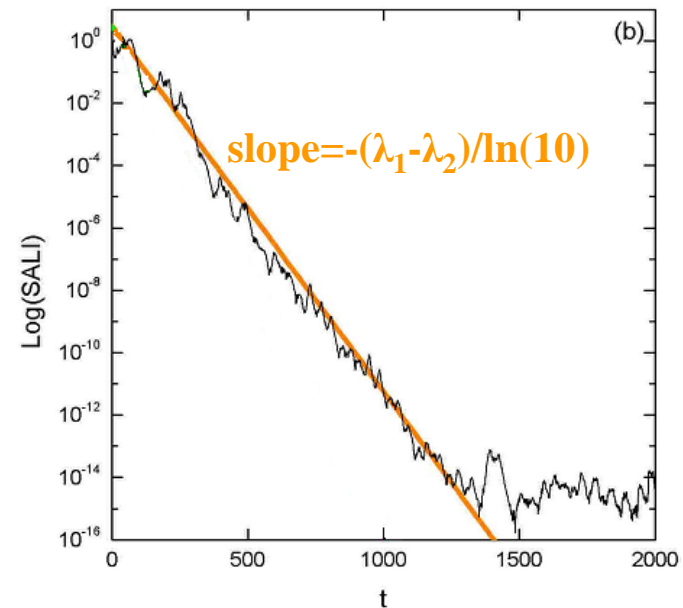
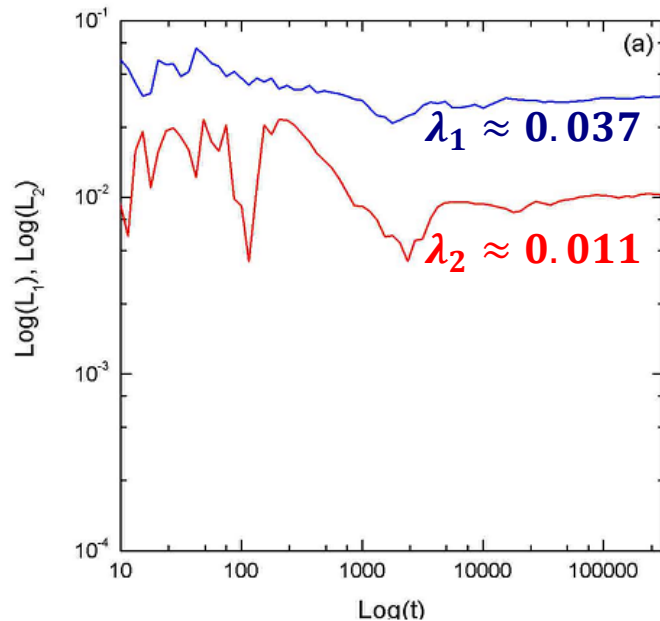


Behavior of the SALI for **chaotic motion**

We test the validity of the approximation $\text{SALI} \propto e^{-(\lambda_1 - \lambda_2)t}$ [S. et al., J. Phys. A (2004)] for a chaotic orbit of the 3D Hamiltonian

$$H = \sum_{i=1}^3 \frac{\omega_i}{2} (q_i^2 + p_i^2) + q_1^2 q_2 + q_1^2 q_3$$

with $\omega_1=1$, $\omega_2=1.4142$, $\omega_3=1.7321$, $H=0.09$

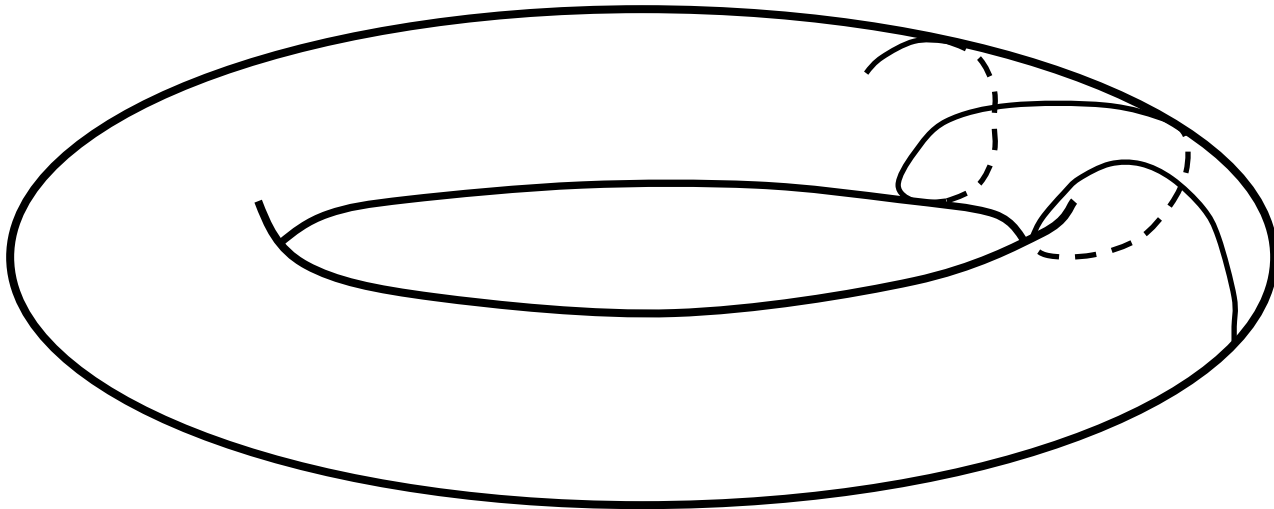


Behavior of SALI for **regular motion**

Regular motion occurs on a torus and two different initial deviation vectors **become tangent to the torus, generally having different directions.**

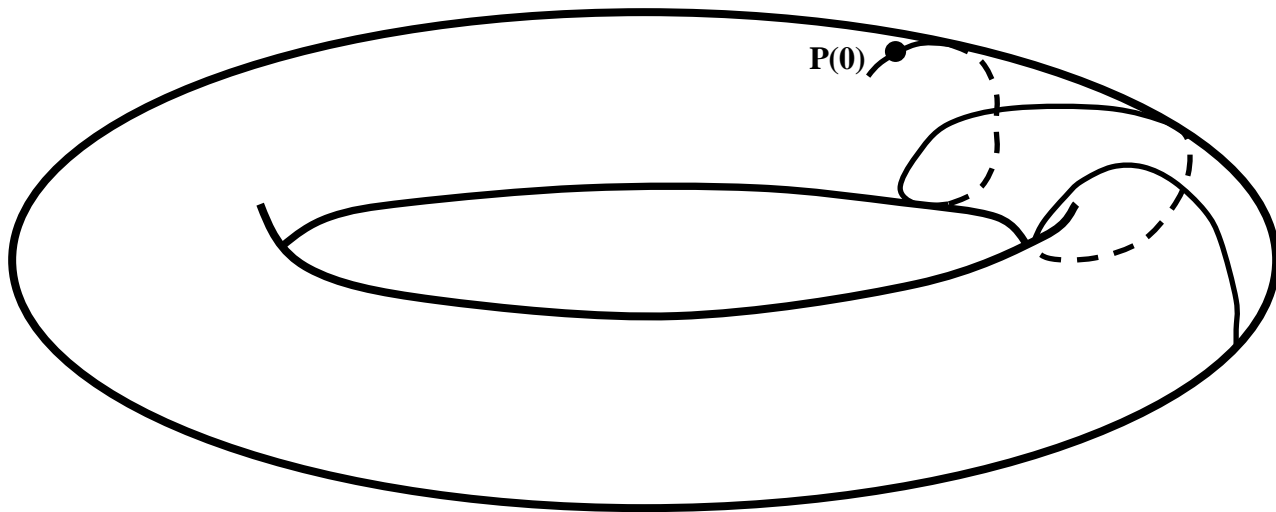
Behavior of SALI for **regular motion**

Regular motion occurs on a torus and two different initial deviation vectors **become tangent to the torus, generally having different directions.**



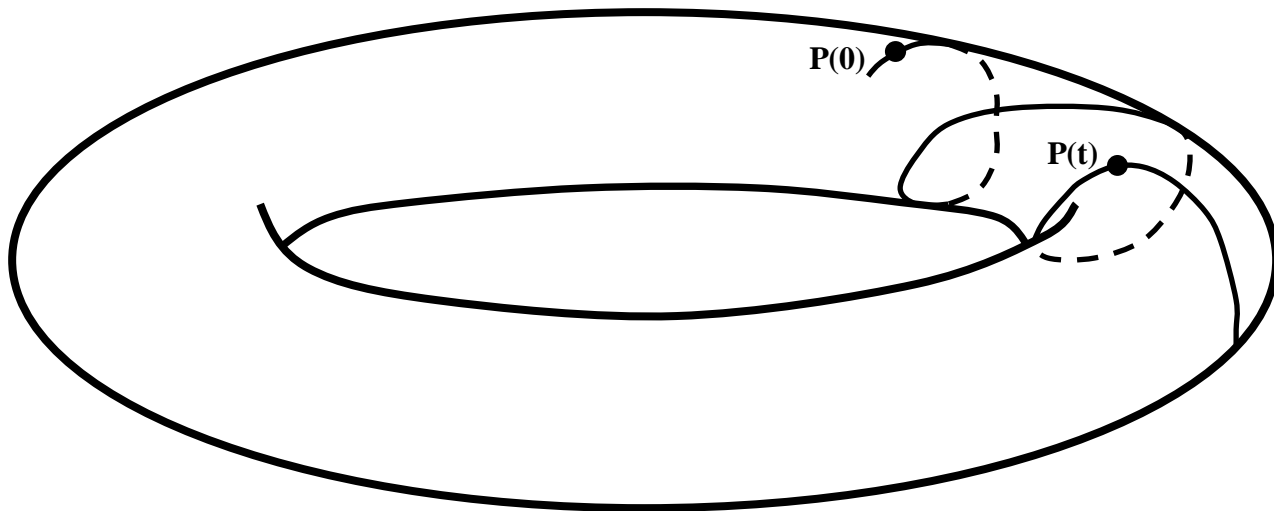
Behavior of SALI for **regular motion**

Regular motion occurs on a torus and two different initial deviation vectors **become tangent to the torus, generally having different directions.**



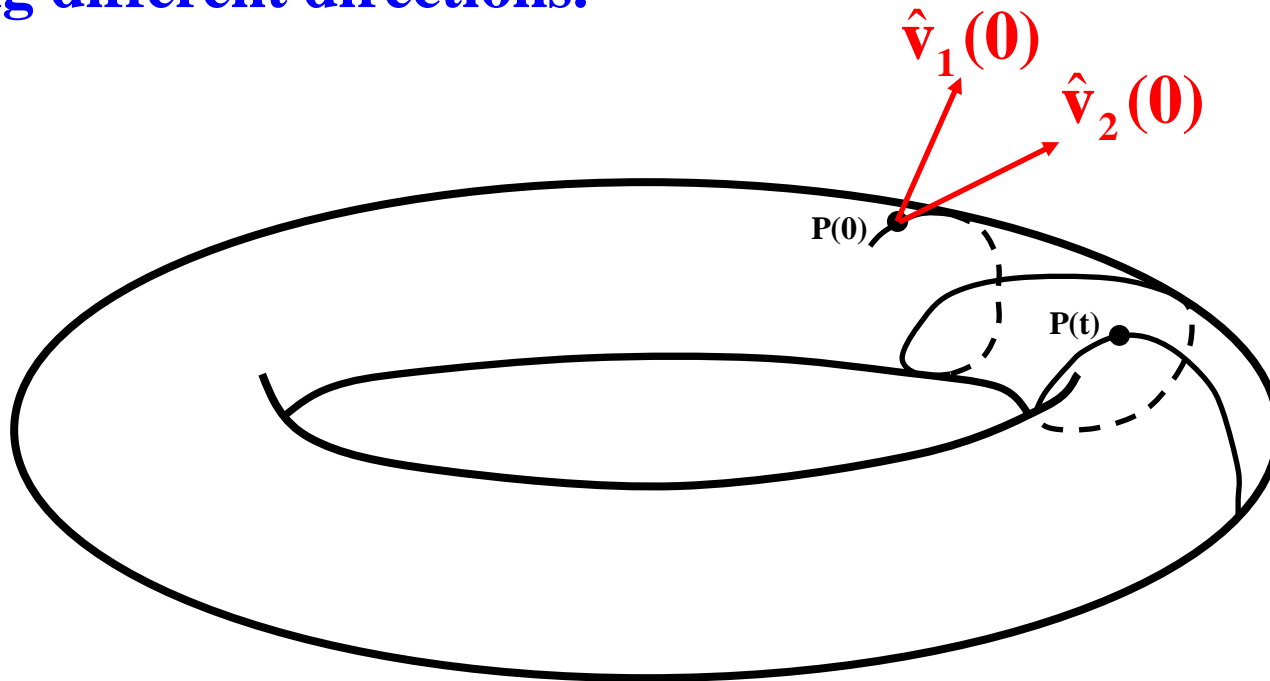
Behavior of SALI for **regular motion**

Regular motion occurs on a torus and two different initial deviation vectors **become tangent to the torus, generally having different directions.**



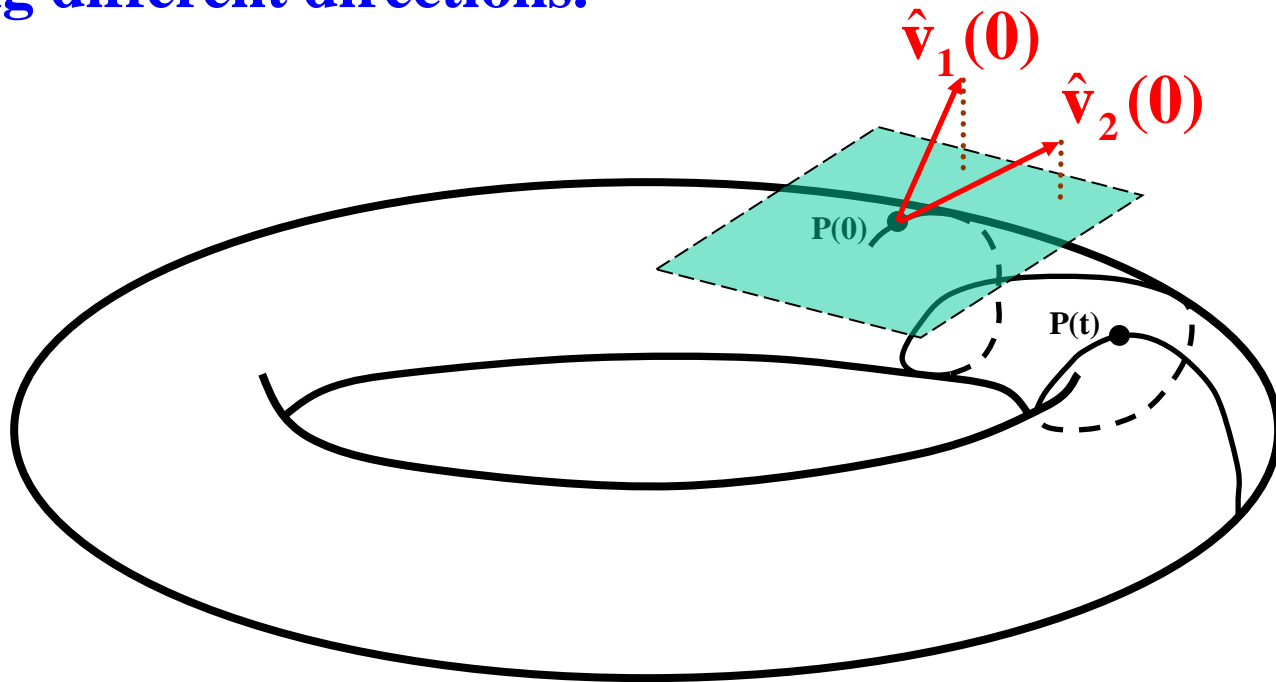
Behavior of SALI for **regular motion**

Regular motion occurs on a torus and two different initial deviation vectors **become tangent to the torus, generally having different directions.**



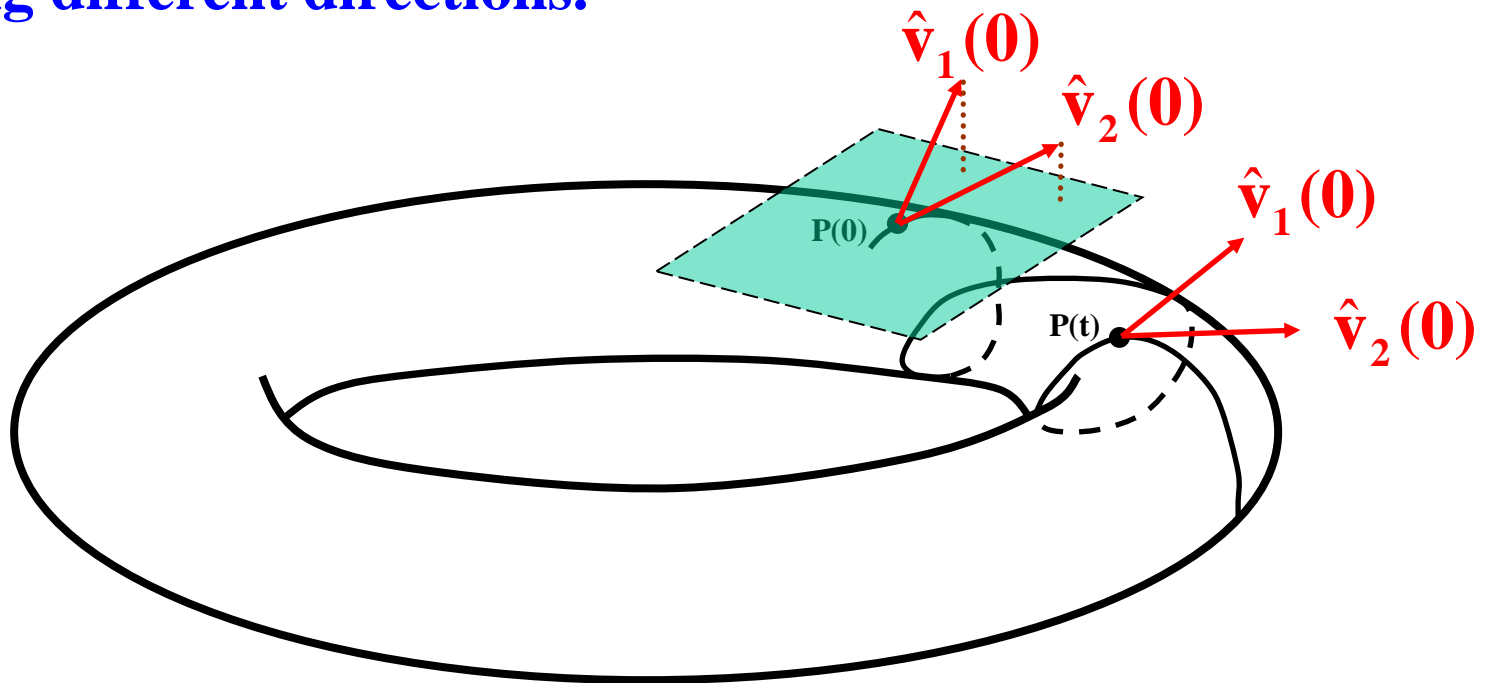
Behavior of SALI for **regular motion**

Regular motion occurs on a torus and two different initial deviation vectors **become tangent to the torus, generally having different directions.**



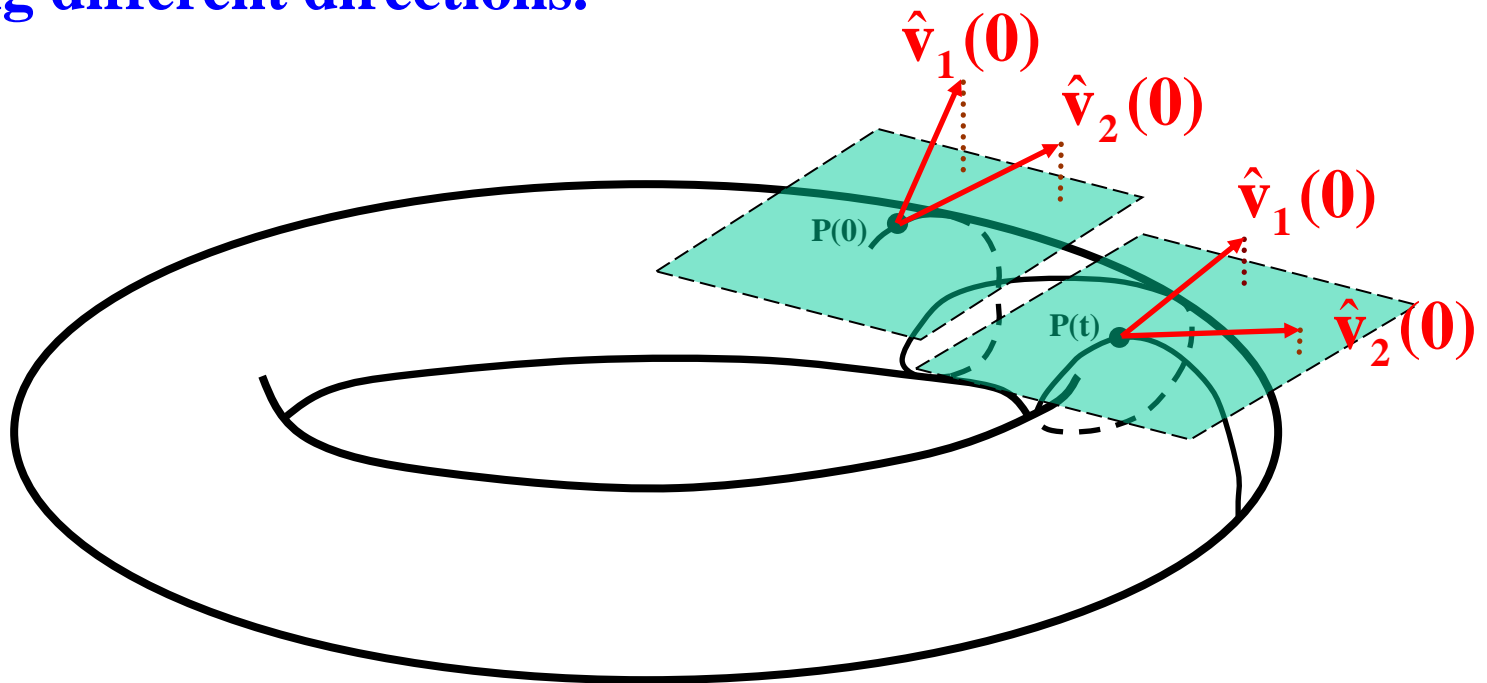
Behavior of SALI for **regular motion**

Regular motion occurs on a torus and two different initial deviation vectors **become tangent to the torus, generally having different directions.**



Behavior of SALI for **regular motion**

Regular motion occurs on a torus and two different initial deviation vectors **become tangent to the torus, generally having different directions.**



SALI – Hénon-Heiles system

As an example, we consider the 2D Hénon-Heiles system:

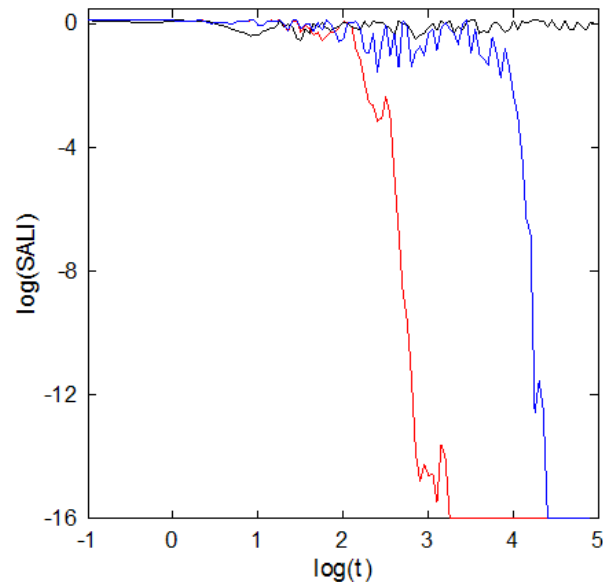
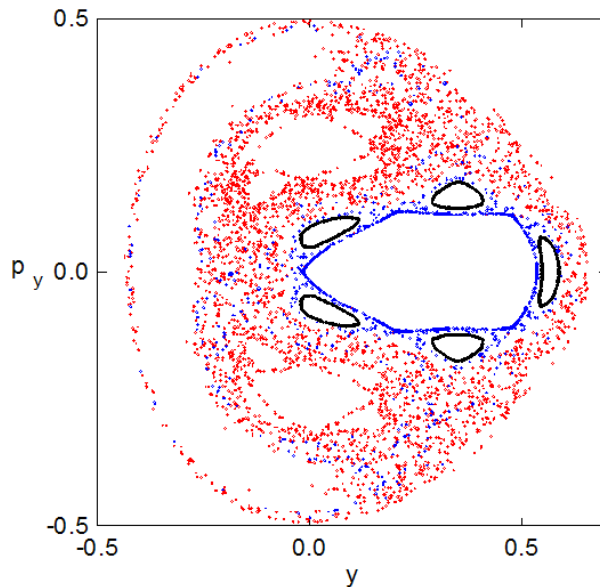
$$H = \frac{1}{2}(p_x^2 + p_y^2) + \frac{1}{2}(x^2 + y^2) + x^2y - \frac{1}{3}y^3$$

For $E=1/8$ we consider the orbits with initial conditions:

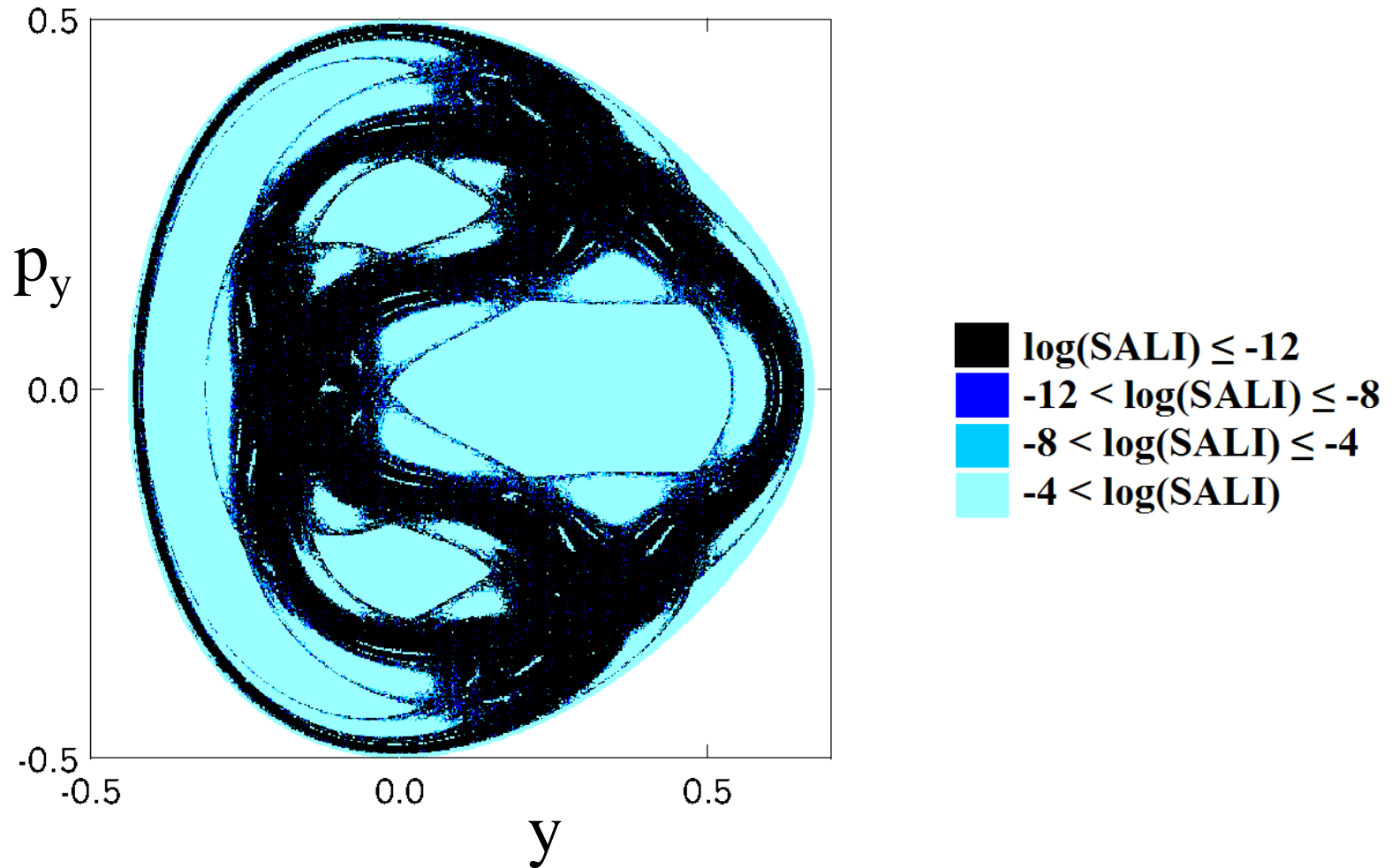
Regular orbit, $x=0$, $y=0.55$, $p_x=0.2417$, $p_y=0$

Chaotic orbit, $x=0$, $y=-0.016$, $p_x=0.49974$, $p_y=0$

Chaotic orbit, $x=0$, $y=-0.01344$, $p_x=0.49982$, $p_y=0$



SALI – Hénon-Heiles system



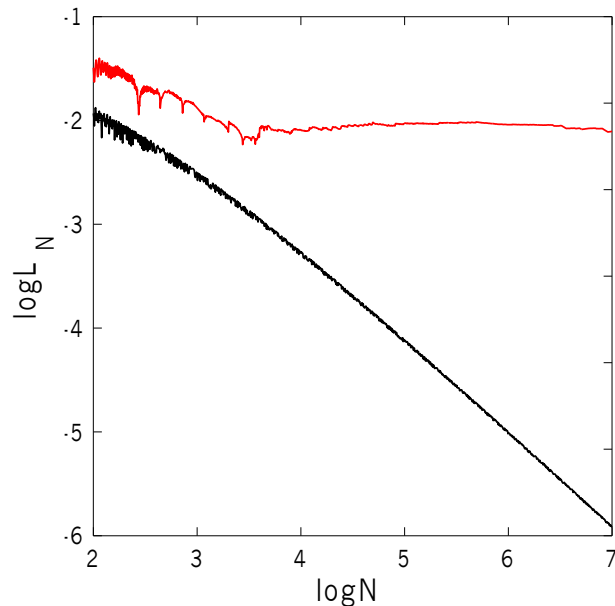
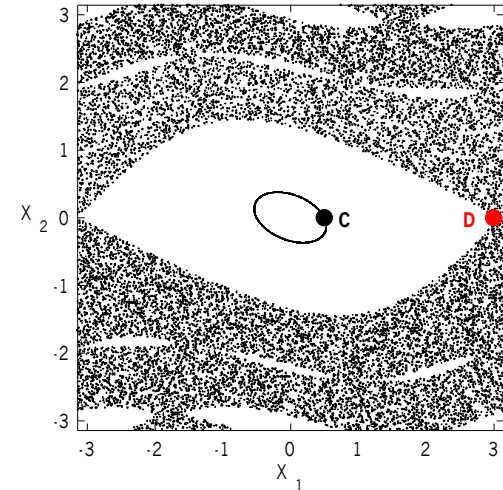
Applications – 4D map

$$\begin{aligned}
 \mathbf{x}'_1 &= \mathbf{x}_1 + \mathbf{x}_2 \\
 \mathbf{x}'_2 &= \mathbf{x}_2 - \nu \sin(\mathbf{x}_1 + \mathbf{x}_2) - \mu [1 - \cos(\mathbf{x}_1 + \mathbf{x}_2 + \mathbf{x}_3 + \mathbf{x}_4)] \\
 \mathbf{x}'_3 &= \mathbf{x}_3 + \mathbf{x}_4 \\
 \mathbf{x}'_4 &= \mathbf{x}_4 - \kappa \sin(\mathbf{x}_3 + \mathbf{x}_4) - \mu [1 - \cos(\mathbf{x}_1 + \mathbf{x}_2 + \mathbf{x}_3 + \mathbf{x}_4)]
 \end{aligned}
 \pmod{2\pi}$$

For $\nu=0.5$, $\kappa=0.1$, $\mu=0.1$ we consider the orbits:

regular orbit C with initial conditions $x_1=0.5$, $x_2=0$, $x_3=0.5$, $x_4=0$.

chaotic orbit D with initial conditions $x_1=3$, $x_2=0$, $x_3=0.5$, $x_4=0$.



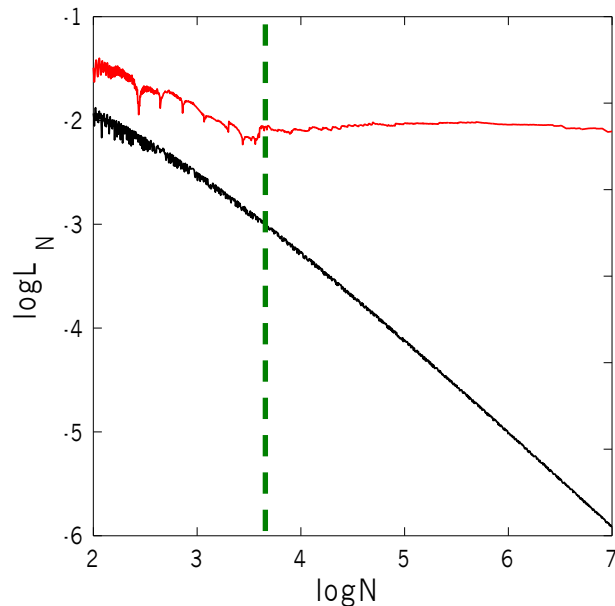
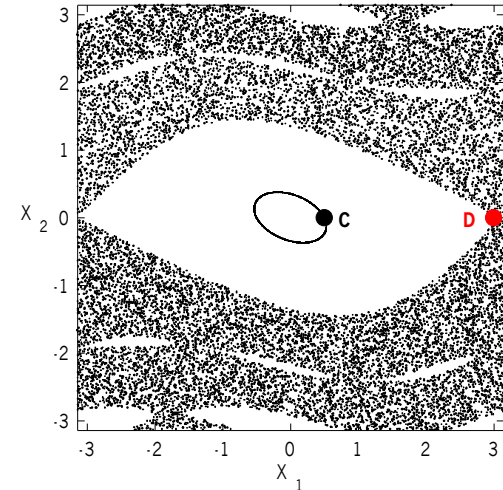
Applications – 4D map

$$\begin{aligned}
 \mathbf{x}'_1 &= \mathbf{x}_1 + \mathbf{x}_2 \\
 \mathbf{x}'_2 &= \mathbf{x}_2 - \nu \sin(\mathbf{x}_1 + \mathbf{x}_2) - \mu [1 - \cos(\mathbf{x}_1 + \mathbf{x}_2 + \mathbf{x}_3 + \mathbf{x}_4)] \\
 \mathbf{x}'_3 &= \mathbf{x}_3 + \mathbf{x}_4 \\
 \mathbf{x}'_4 &= \mathbf{x}_4 - \kappa \sin(\mathbf{x}_3 + \mathbf{x}_4) - \mu [1 - \cos(\mathbf{x}_1 + \mathbf{x}_2 + \mathbf{x}_3 + \mathbf{x}_4)]
 \end{aligned}
 \pmod{2\pi}$$

For $\nu=0.5$, $\kappa=0.1$, $\mu=0.1$ we consider the orbits:

regular orbit C with initial conditions $x_1=0.5$, $x_2=0$, $x_3=0.5$, $x_4=0$.

chaotic orbit D with initial conditions $x_1=3$, $x_2=0$, $x_3=0.5$, $x_4=0$.



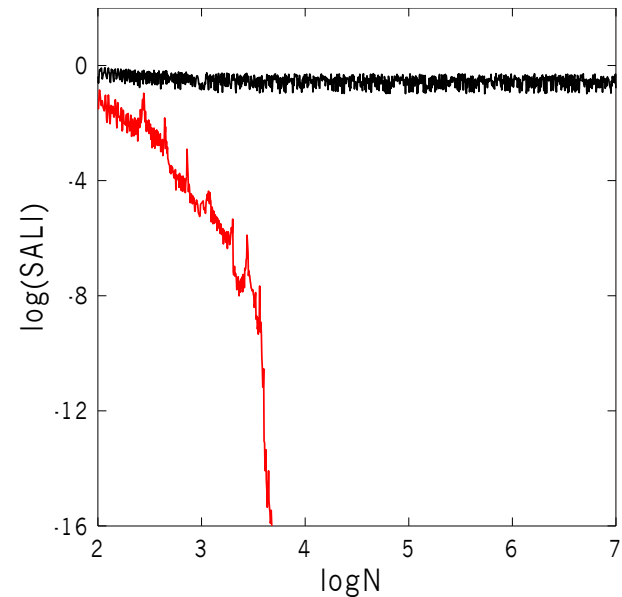
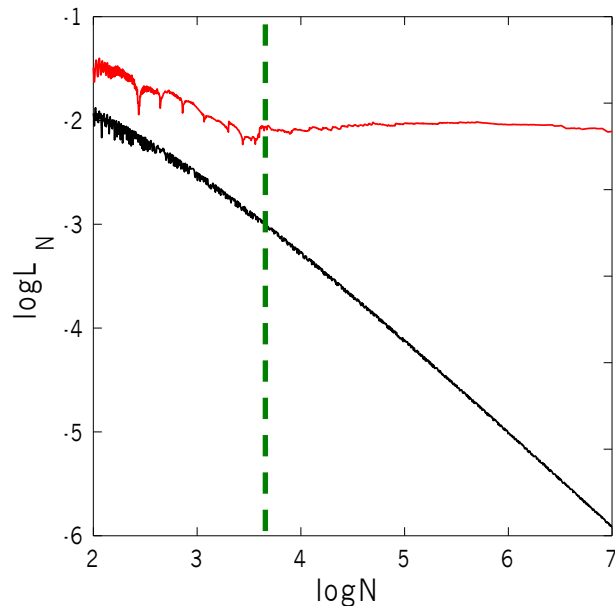
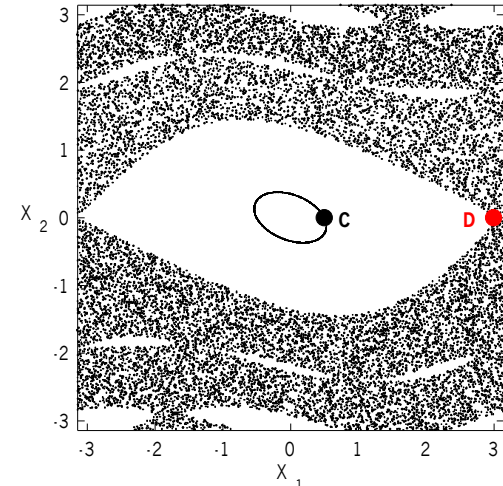
Applications – 4D map

$$\begin{aligned}
 \mathbf{x}'_1 &= \mathbf{x}_1 + \mathbf{x}_2 \\
 \mathbf{x}'_2 &= \mathbf{x}_2 - \nu \sin(\mathbf{x}_1 + \mathbf{x}_2) - \mu [1 - \cos(\mathbf{x}_1 + \mathbf{x}_2 + \mathbf{x}_3 + \mathbf{x}_4)] \\
 \mathbf{x}'_3 &= \mathbf{x}_3 + \mathbf{x}_4 \\
 \mathbf{x}'_4 &= \mathbf{x}_4 - \kappa \sin(\mathbf{x}_3 + \mathbf{x}_4) - \mu [1 - \cos(\mathbf{x}_1 + \mathbf{x}_2 + \mathbf{x}_3 + \mathbf{x}_4)]
 \end{aligned} \pmod{2\pi}$$

For $\nu=0.5$, $\kappa=0.1$, $\mu=0.1$ we consider the orbits:

regular orbit C with initial conditions $x_1=0.5$, $x_2=0$, $x_3=0.5$, $x_4=0$.

chaotic orbit D with initial conditions $x_1=3$, $x_2=0$, $x_3=0.5$, $x_4=0$.



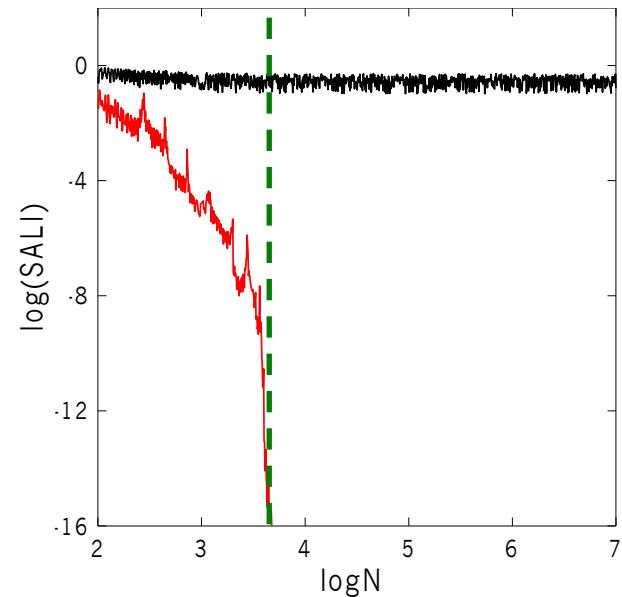
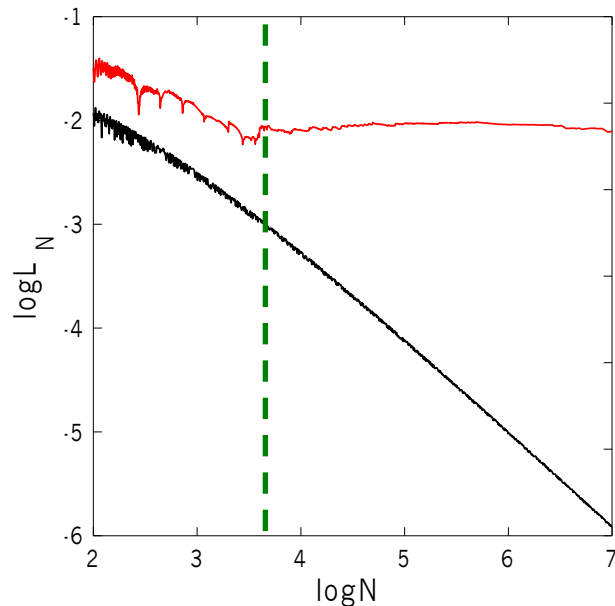
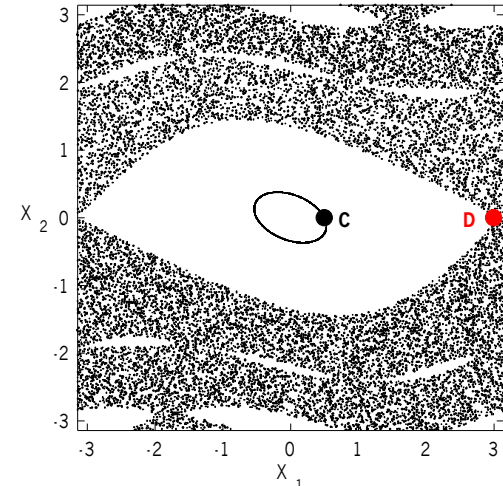
Applications – 4D map

$$\begin{aligned}
 \mathbf{x}'_1 &= \mathbf{x}_1 + \mathbf{x}_2 \\
 \mathbf{x}'_2 &= \mathbf{x}_2 - \nu \sin(\mathbf{x}_1 + \mathbf{x}_2) - \mu [1 - \cos(\mathbf{x}_1 + \mathbf{x}_2 + \mathbf{x}_3 + \mathbf{x}_4)] \\
 \mathbf{x}'_3 &= \mathbf{x}_3 + \mathbf{x}_4 \\
 \mathbf{x}'_4 &= \mathbf{x}_4 - \kappa \sin(\mathbf{x}_3 + \mathbf{x}_4) - \mu [1 - \cos(\mathbf{x}_1 + \mathbf{x}_2 + \mathbf{x}_3 + \mathbf{x}_4)]
 \end{aligned}
 \pmod{2\pi}$$

For $\nu=0.5$, $\kappa=0.1$, $\mu=0.1$ we consider the orbits:

regular orbit C with initial conditions $x_1=0.5$, $x_2=0$, $x_3=0.5$, $x_4=0$.

chaotic orbit D with initial conditions $x_1=3$, $x_2=0$, $x_3=0.5$, $x_4=0$.



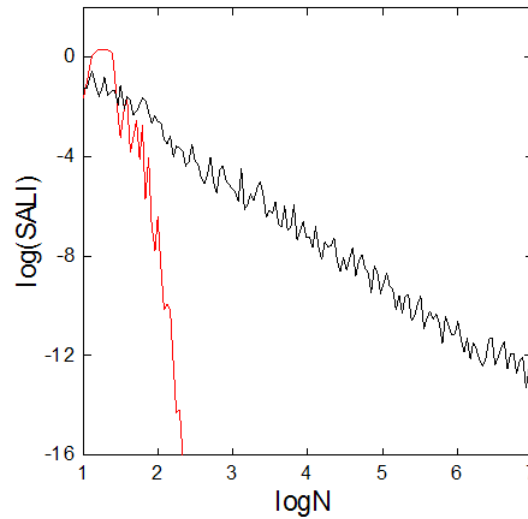
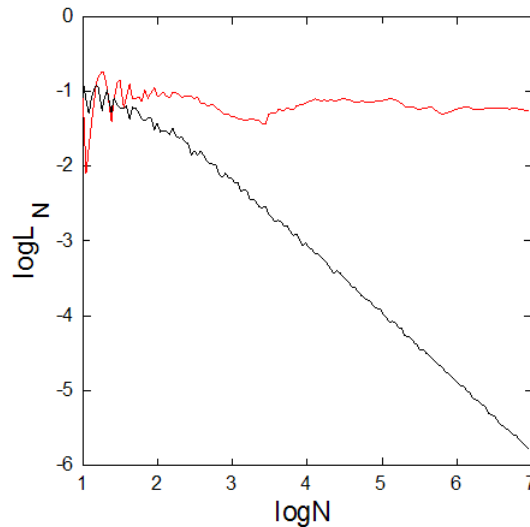
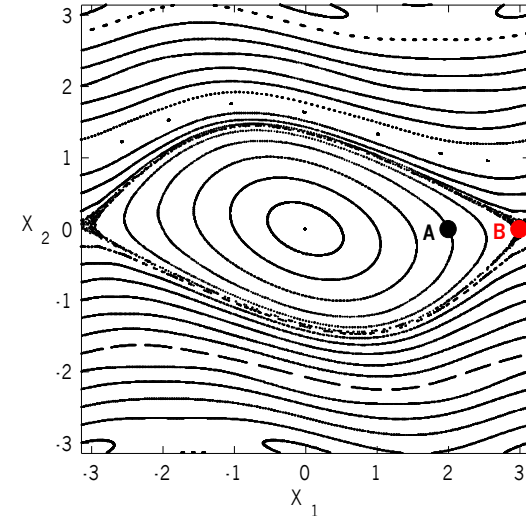
Applications – 2D map

$$\begin{aligned}x_1' &= x_1 + x_2 \\x_2' &= x_2 - \nu \sin(x_1 + x_2)\end{aligned}\quad (\text{mod } 2\pi)$$

For $\nu=0.5$ we consider the orbits:

regular orbit A with initial conditions $x_1=2, x_2=0$.

chaotic orbit B with initial conditions $x_1=3, x_2=0$.



Behavior of the SALI

2D maps

SALI $\rightarrow 0$ both for regular and chaotic orbits

following, however, completely different time rates which allows us to distinguish between the two cases.

Hamiltonian flows and multidimensional maps

SALI $\rightarrow 0$ for chaotic orbits

SALI \rightarrow constant $\neq 0$ for regular orbits

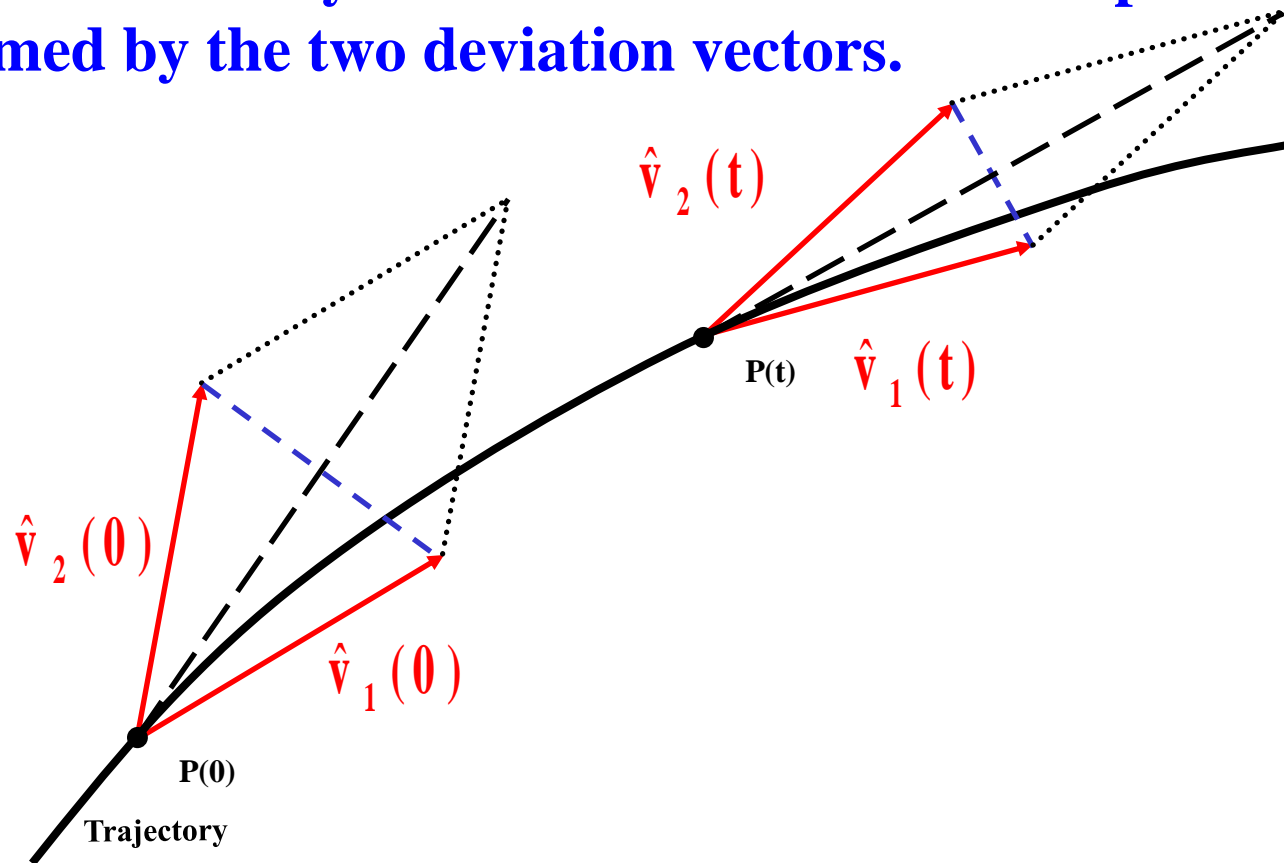
**The
Generalized ALignment Indices
(GALIs)
method**

Definition of the Generalized Alignment Index (GALI)

SALI effectively measures the 'area' of the parallelogram formed by the two deviation vectors.

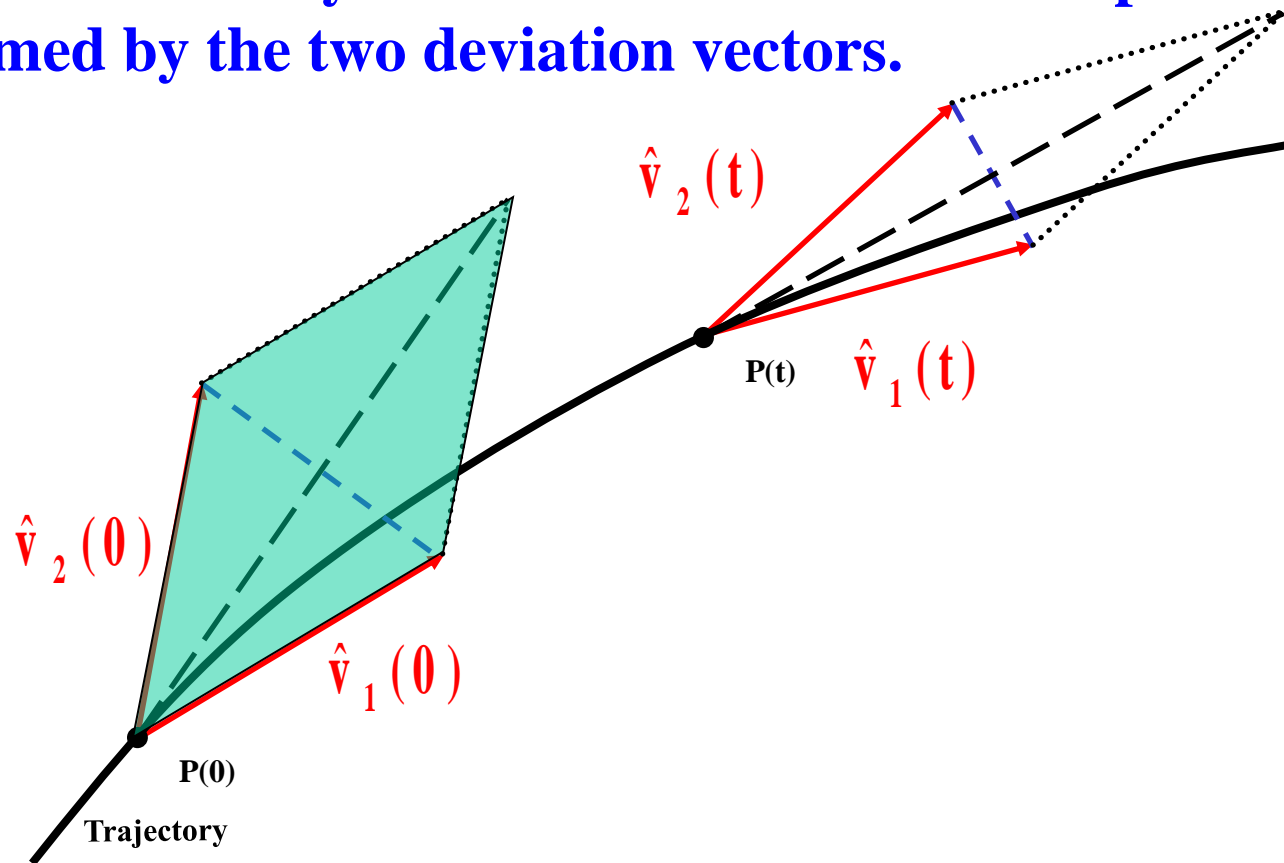
Definition of the Generalized Alignment Index (GALI)

SALI effectively measures the 'area' of the parallelogram formed by the two deviation vectors.



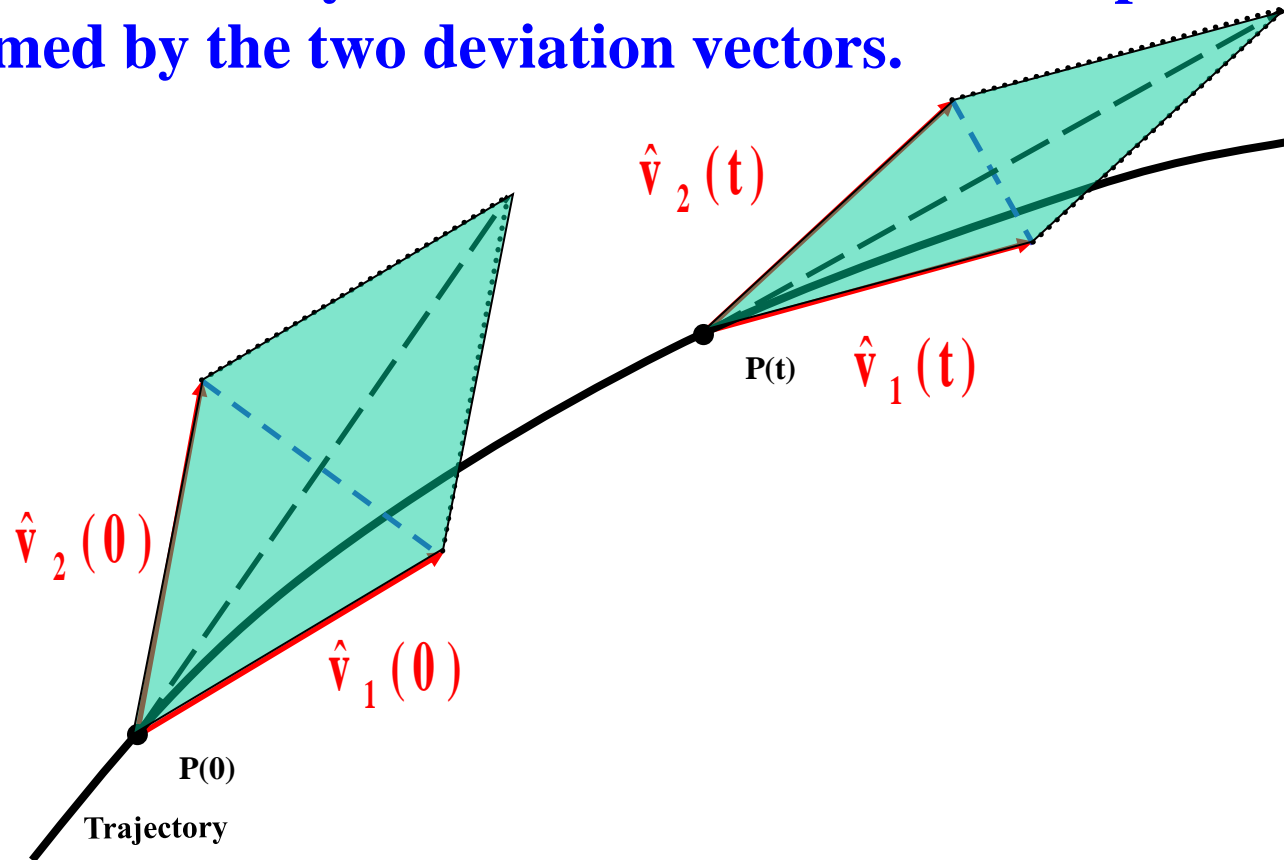
Definition of the Generalized Alignment Index (GALI)

SALI effectively measures the 'area' of the parallelogram formed by the two deviation vectors.



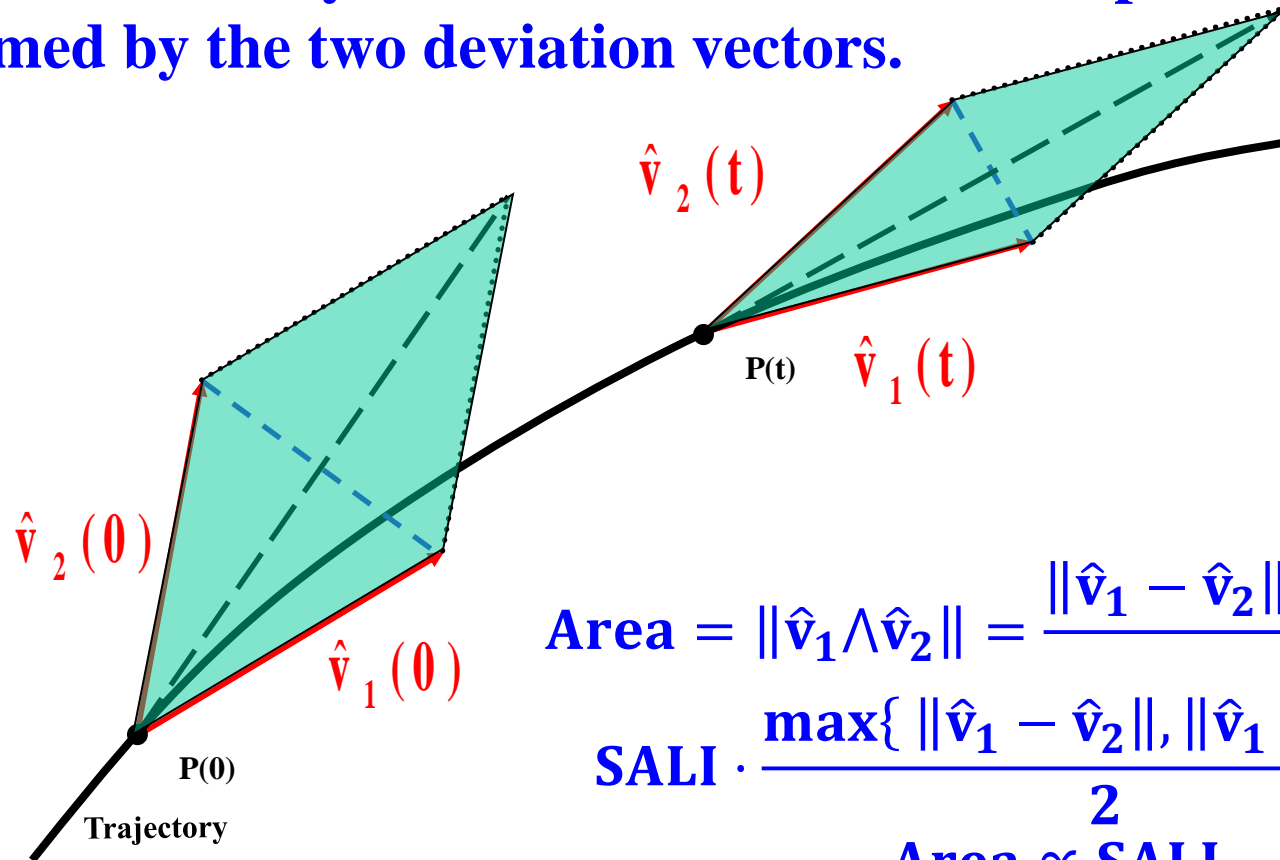
Definition of the Generalized Alignment Index (GALI)

SALI effectively measures the 'area' of the parallelogram formed by the two deviation vectors.



Definition of the Generalized Alignment Index (GALI)

SALI effectively measures the 'area' of the parallelogram formed by the two deviation vectors.



$$\text{Area} = \|\hat{v}_1 \wedge \hat{v}_2\| = \frac{\|\hat{v}_1 - \hat{v}_2\| \cdot \|\hat{v}_1 + \hat{v}_2\|}{2} =$$

$$\text{SALI} \cdot \frac{\max\{\|\hat{v}_1 - \hat{v}_2\|, \|\hat{v}_1 + \hat{v}_2\|\}}{2} \Rightarrow$$

$$\text{Area} \propto \text{SALI}$$

Definition of the Generalized Alignment Index (GALI)

In the case of an N degree of freedom Hamiltonian system we follow the evolution of k deviation vectors with $2 \leq k \leq 2N$, and define [S. et al., Physica D (2007)] the **Generalized Alignment Index (GALI)** of order k :

$$\text{GALI}_k(t) = \|\hat{\mathbf{v}}_1(t) \wedge \hat{\mathbf{v}}_2(t) \wedge \dots \wedge \hat{\mathbf{v}}_k(t)\|$$

where

$$\hat{\mathbf{v}}_1(t) = \frac{\mathbf{v}_1(t)}{\|\mathbf{v}_1(t)\|}.$$

Note that **GALI₂** ($k=2$) is equivalent to the **Smaller Alignment Index (SALI)**.

Behavior of the $GALI_k$

Chaotic motion: $GALI_k$ ($2 \leq k \leq 2N$) tends exponentially to zero with exponents which involve the values of the first k largest Lyapunov exponents $\lambda_1, \lambda_2, \dots, \lambda_k$:

$$GALI_k(t) \propto e^{-[(\lambda_1 - \lambda_2) + (\lambda_1 - \lambda_3) + \dots + (\lambda_1 - \lambda_k)]t}$$

Regular motion: When the motion occurs on an N -dimensional torus then the behavior of $GALI_k$ is given by [S. et al., Physica D (2007) – S. et al., Eur. Phys. J. Sp. Top. (2008)]:

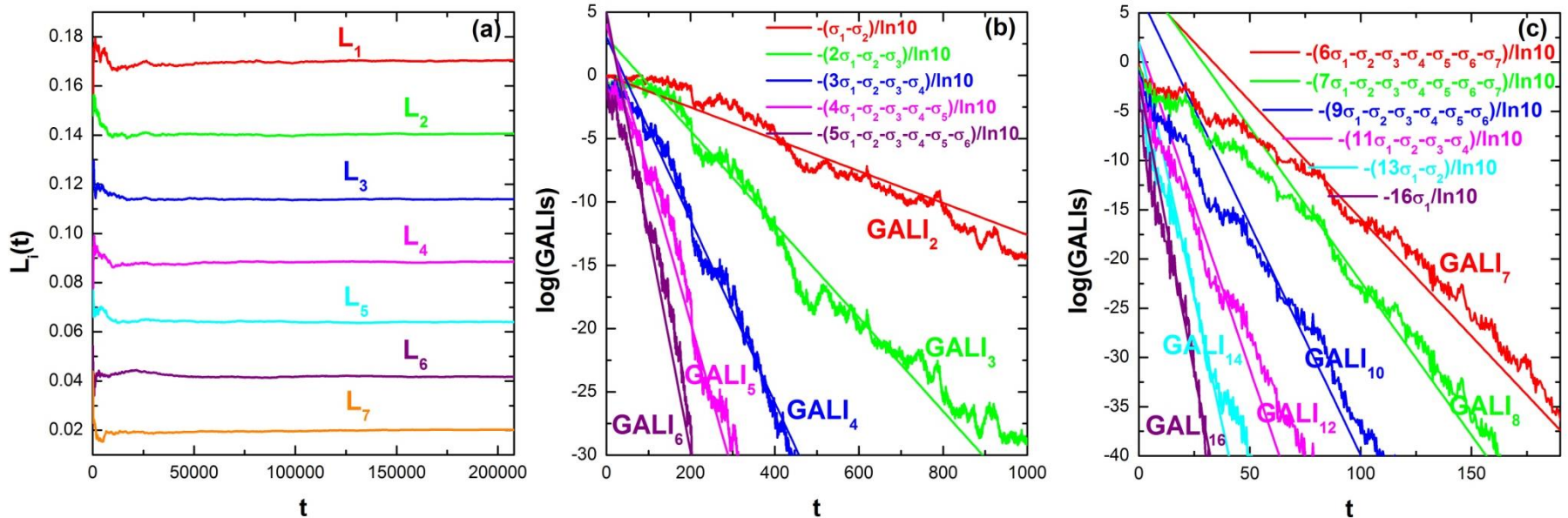
$$GALI_k(t) \propto \begin{cases} \text{constant} & \text{if } 2 \leq k \leq N \\ \frac{1}{t^{2(k-N)}} & \text{if } N < k \leq 2N \end{cases}$$

Behavior of the $GALI_k$ for **chaotic motion**

N particles Fermi-Pasta-Ulam-Tsingou (FPUT) system:

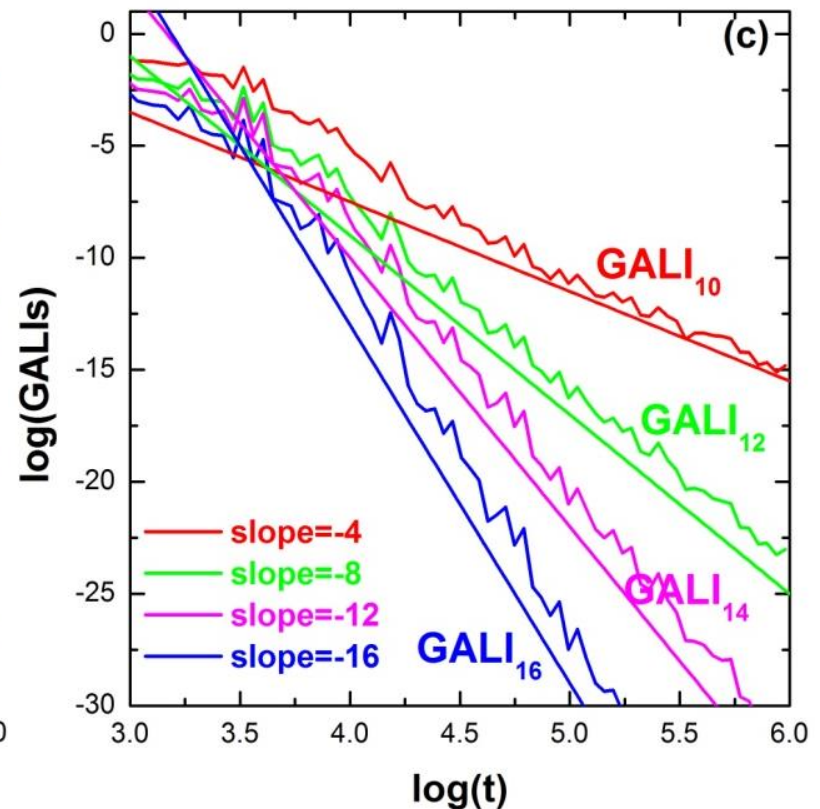
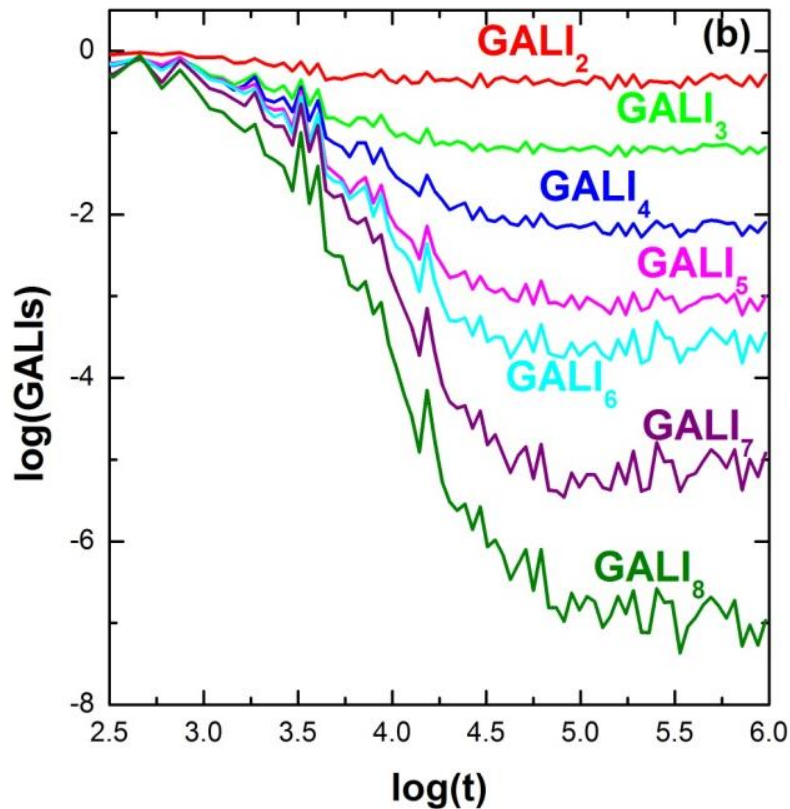
$$H = \frac{1}{2} \sum_{i=1}^N p_i^2 + \sum_{i=0}^N \left[\frac{1}{2} (q_{i+1} - q_i)^2 + \frac{\beta}{4} (q_{i+1} - q_i)^4 \right]$$

with fixed boundary conditions, $N=8$ and $\beta=1.5$.



Behavior of the $GALI_k$ for regular motion

N=8 FPUT system



Global dynamics

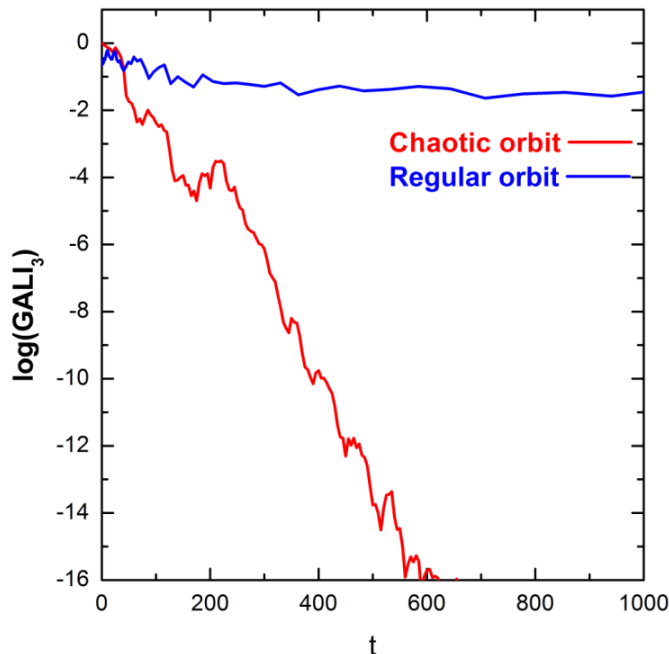
- $GALI_2$ (practically equivalent to the use of SALI)

- $GALI_N$

Chaotic motion: $GALI_N \rightarrow 0$
(exponential decay)

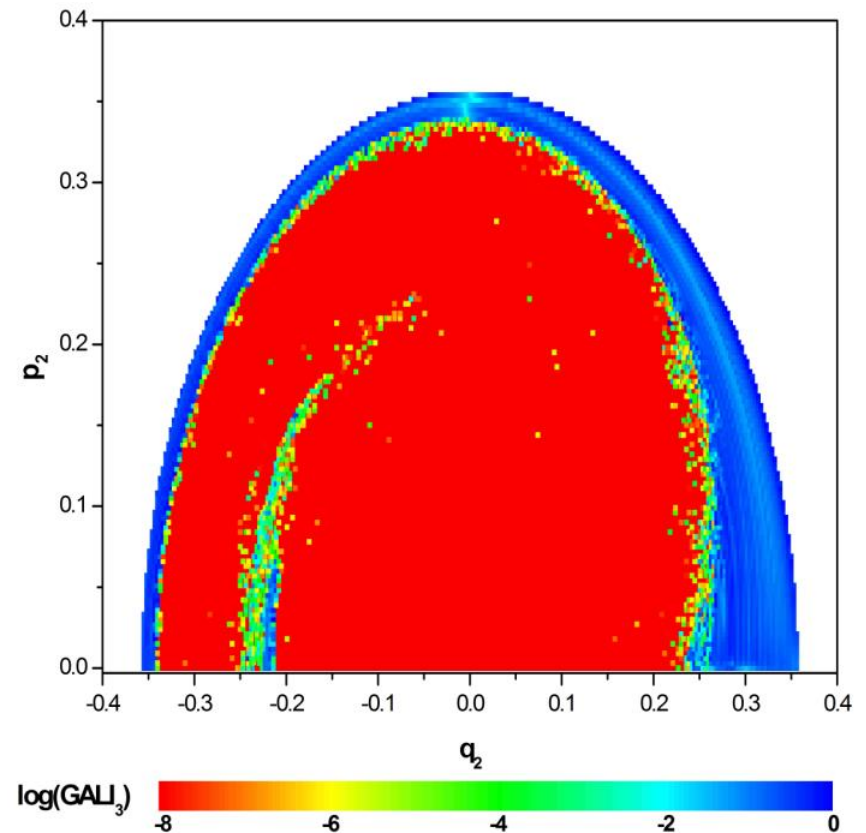
Regular motion:

$GALI_N \approx \text{constant} \neq 0$



3D Hamiltonian

Subspace $q_3=p_3=0$, $p_2 \geq 0$ for $t=1000$.



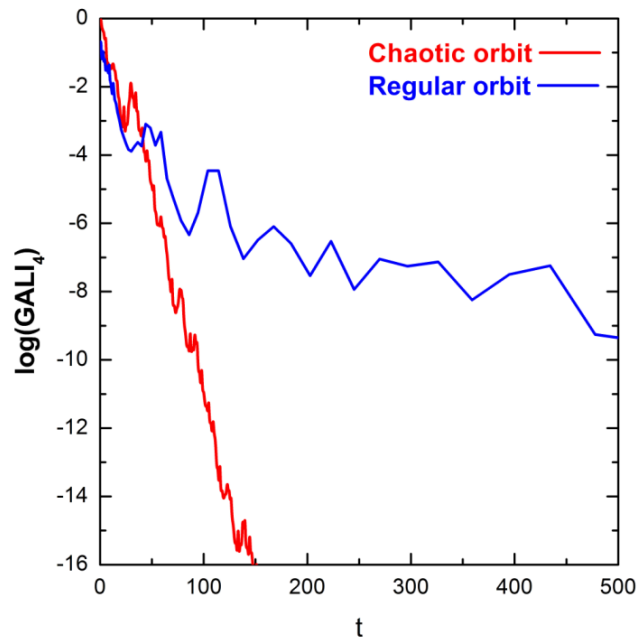
Global dynamics

$GALI_k$ with $k > N$

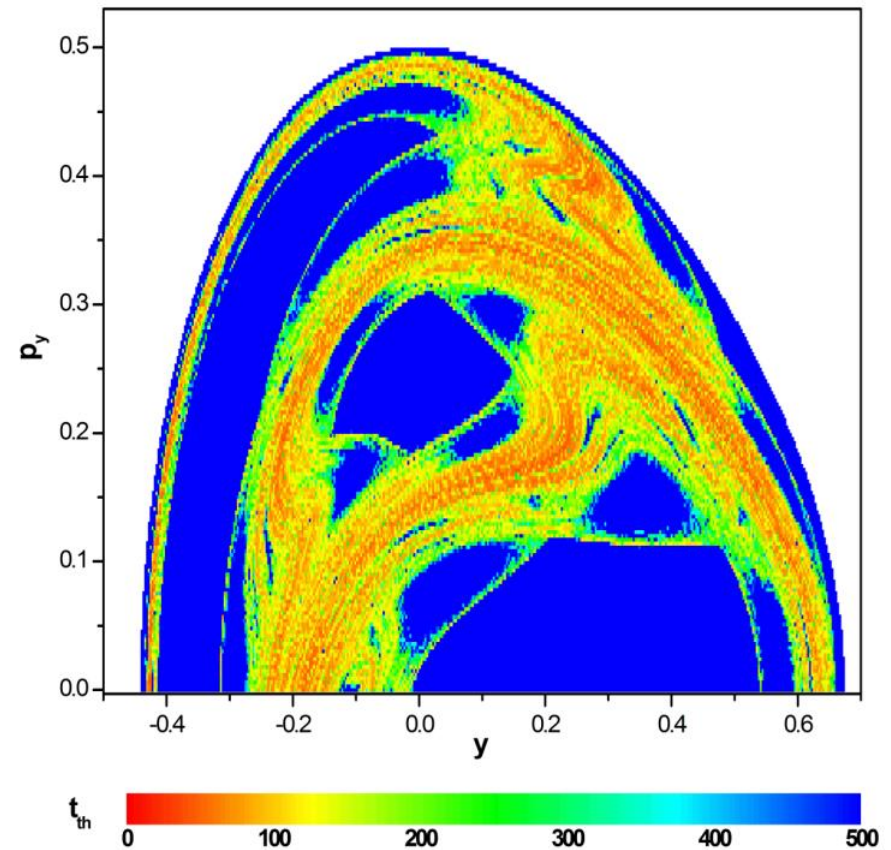
The index tends to zero both for regular and chaotic orbits but with completely different time rates:

Chaotic motion: exponential decay

Regular motion: power law



2D Hamiltonian (Hénon-Heiles) Time needed for $GALI_4 < 10^{-12}$



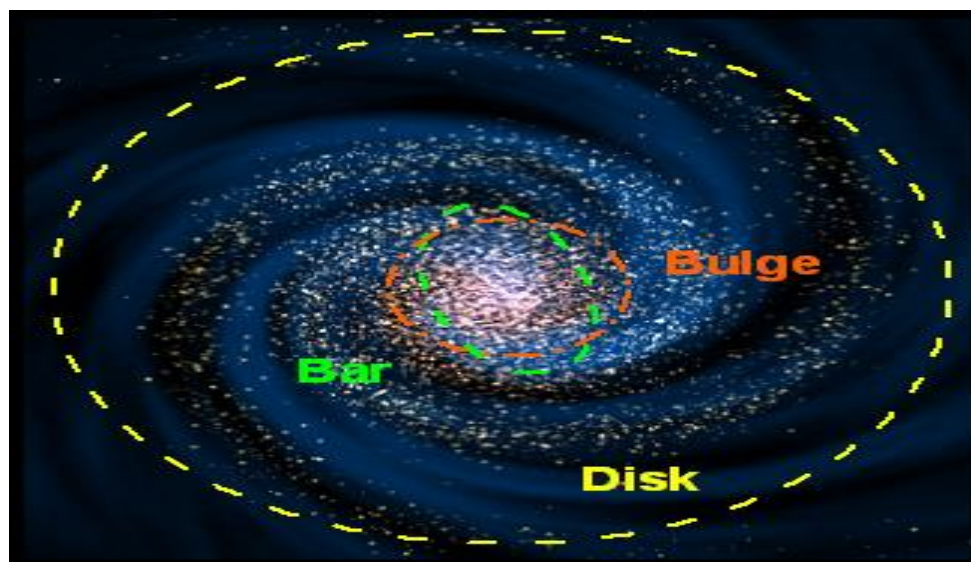
A time-dependent Hamiltonian system

Barred galaxies

NGC 1433



NGC 2217



Barred galaxy model

The 3D bar rotates around its short z -axis (x : long axis and y : intermediate). The Hamiltonian that describes the motion for this model is:

$$H = \frac{1}{2}(p_x^2 + p_y^2 + p_z^2) + V(x, y, z) - \Omega_b(xp_y - yp_x) \equiv \text{Energy}$$

This model consists of the superposition of potentials describing an **axisymmetric** part and a **bar** component of the galaxy [Manos et al., J. Phys. A (2013)].

a) Axisymmetric component:

i) Plummer sphere:

$$V_{\text{sphere}}(x, y, z) = -\frac{GM_S}{\sqrt{x^2 + y^2 + z^2 + \epsilon_s^2}}$$

ii) Miyamoto–Nagai disc:

$$V_{\text{disc}}(x, y, z) = -\frac{GM_D}{\sqrt{x^2 + y^2 + (A + \sqrt{B^2 + z^2})^2}}$$

b) Bar component: $V_{\text{bar}}(x, y, z) = -\pi Gabc \frac{\rho_c}{n+1} \int_{\lambda}^{\infty} \frac{du}{\Delta(u)} (1 - m^2(u))^{n+1}$,

(Ferrers bar)

$$\rho_c = \frac{105}{32\pi} \frac{GM_B}{abc}$$

where $m^2(u) = \frac{x^2}{a^2 + u} + \frac{y^2}{b^2 + u} + \frac{z^2}{c^2 + u}$, $\Delta^2(u) = (a^2 + u)(b^2 + u)(c^2 + u)$,

n : positive integer ($n = 2$ for our model), λ : the unique positive solution of $m^2(\lambda) = 1$

Its density is:

$$\rho = \begin{cases} \rho_c (1 - m^2)^n, & \text{for } m \leq 1 \\ 0, & \text{for } m > 1 \end{cases}, \text{ where } m^2 = \frac{x^2}{a^2} + \frac{y^2}{b^2} + \frac{z^2}{c^2}, \text{ } a > b > c \text{ and } n = 2.$$

Time-dependent barred galaxy model

The 3D bar rotates around its short z -axis (x : long axis and y : intermediate). The Hamiltonian that describes the motion for this model is:

$$H = \frac{1}{2}(p_x^2 + p_y^2 + p_z^2) + V(x, y, z, t) - \Omega_b(xp_y - yp_x) \equiv \text{Energy}$$

This model consists of the superposition of potentials describing an **axisymmetric** part and a **bar** component of the galaxy [Manos et al., J. Phys. A (2013)].

a) Axisymmetric component:

$$M_S + M_B(t) + M_D(t) = 1, \text{ with } M_B(t) = M_B(0) + \alpha t$$

i) Plummer sphere:

$$V_{\text{sphere}}(x, y, z) = -\frac{GM_S}{\sqrt{x^2 + y^2 + z^2 + \epsilon_s^2}}$$

ii) Miyamoto–Nagai disc:

$$V_{\text{disc}}(x, y, z) = -\frac{GM_D(t)}{\sqrt{x^2 + y^2 + (A + \sqrt{B^2 + z^2})^2}}$$

b) Bar component: $V_{\text{bar}}(x, y, z) = -\pi Gabc \frac{\rho_c}{n+1} \int_{\lambda}^{\infty} \frac{du}{\Delta(u)} (1 - m^2(u))^{n+1}$,

(Ferrers bar)

$$\rho_c = \frac{105}{32\pi} \frac{GM_B(t)}{abc}$$

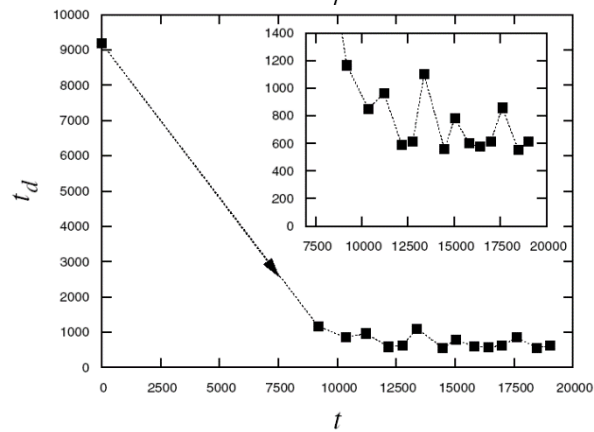
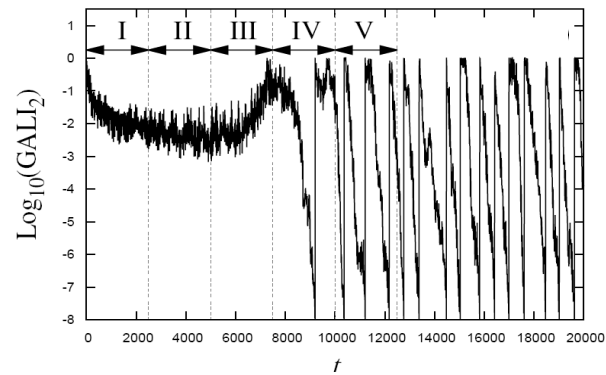
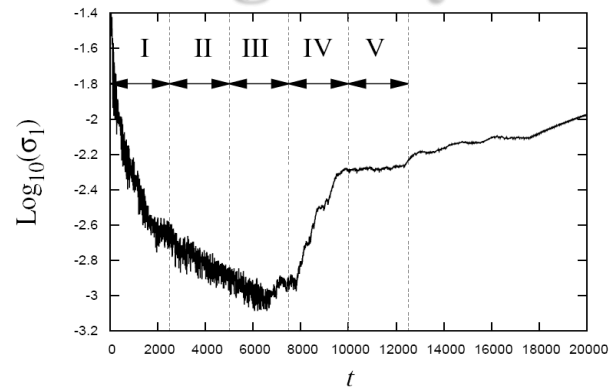
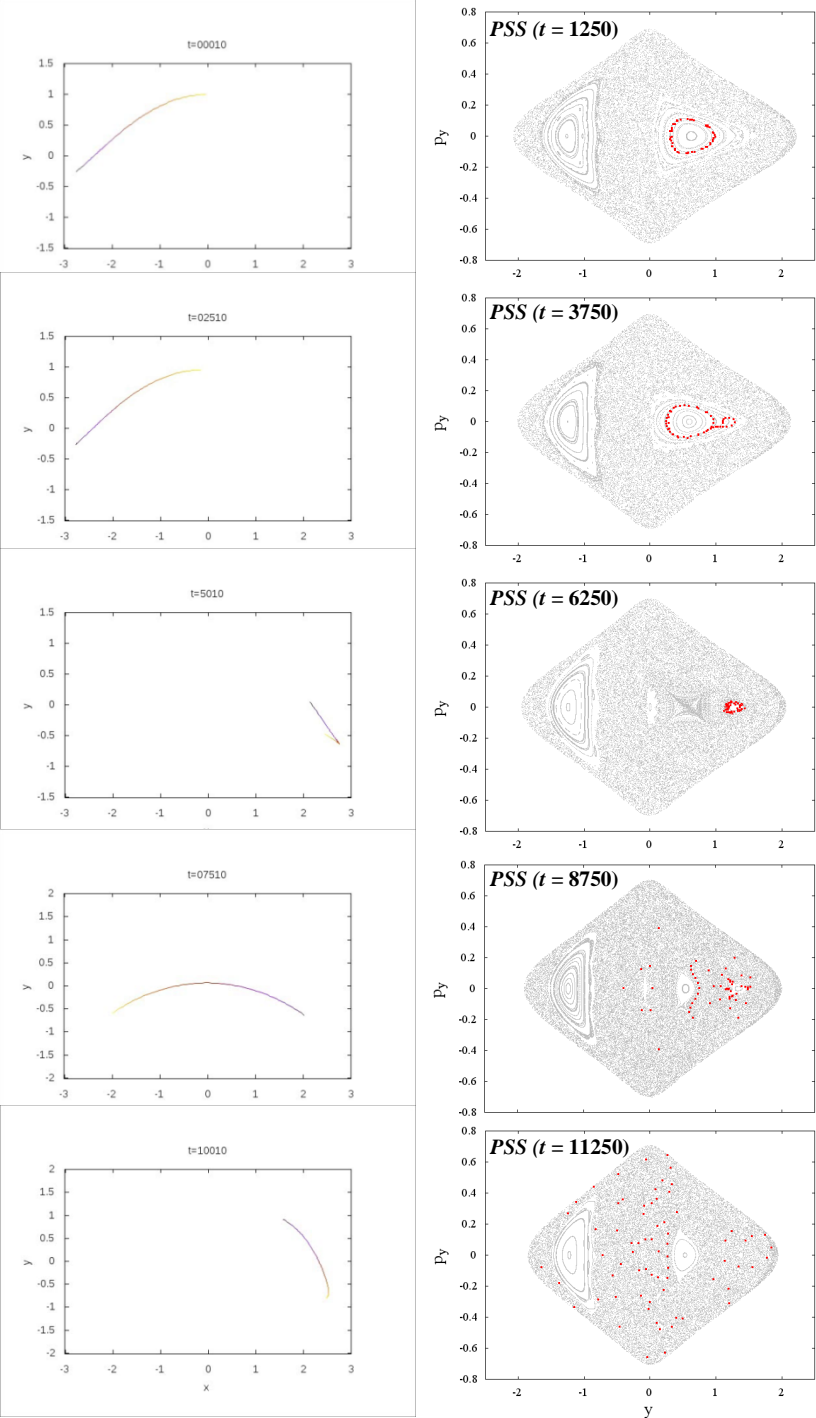
where $m^2(u) = \frac{x^2}{a^2 + u} + \frac{y^2}{b^2 + u} + \frac{z^2}{c^2 + u}$, $\Delta^2(u) = (a^2 + u)(b^2 + u)(c^2 + u)$,

n : positive integer ($n = 2$ for our model), λ : the unique positive solution of $m^2(\lambda) = 1$

Its density is:

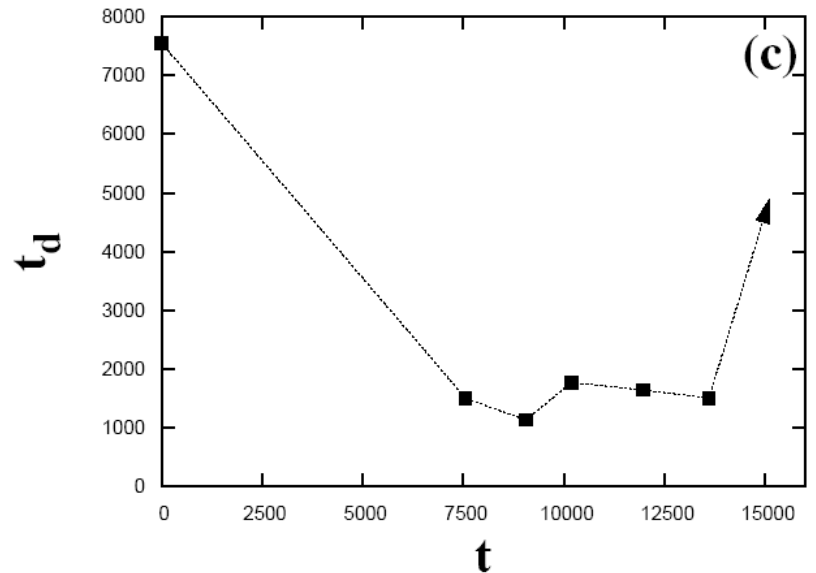
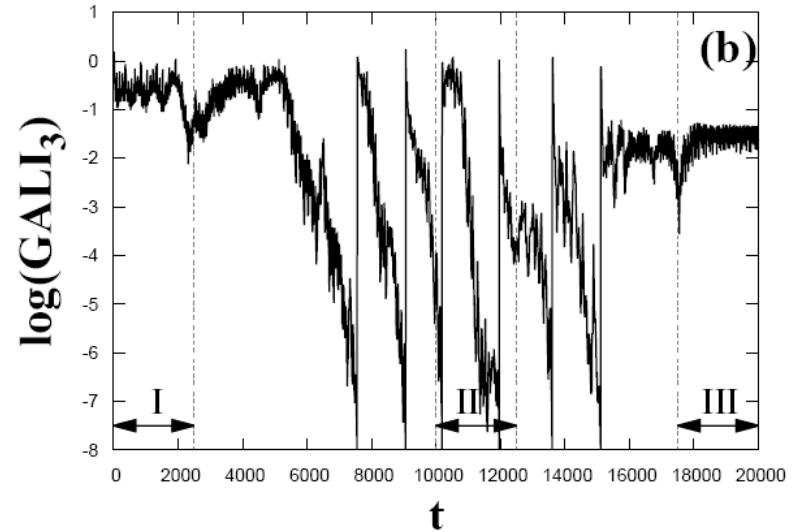
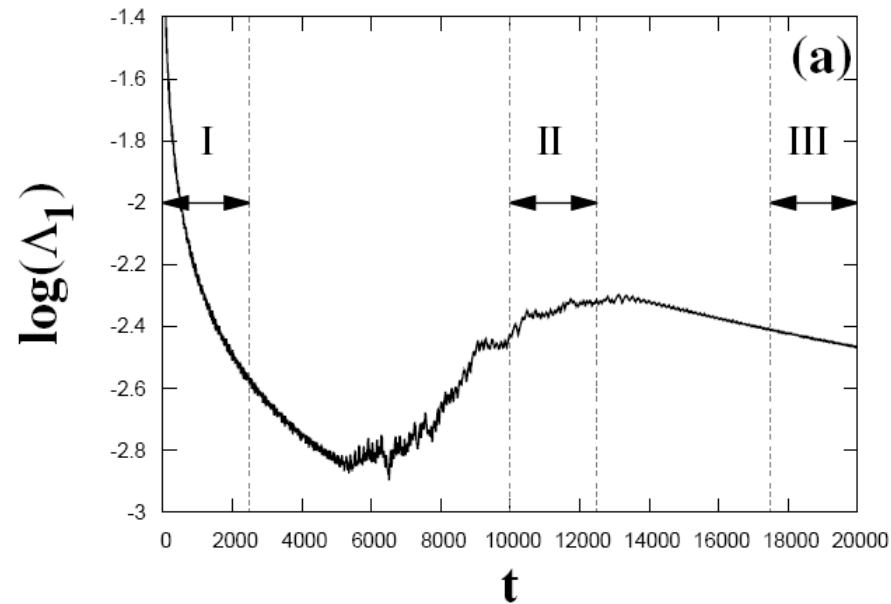
$$\rho = \begin{cases} \rho_c (1 - m^2)^n, & \text{for } m \leq 1 \\ 0, & \text{for } m > 1 \end{cases}, \text{ where } m^2 = \frac{x^2}{a^2} + \frac{y^2}{b^2} + \frac{z^2}{c^2}, \text{ } a > b > c \text{ and } n = 2.$$

Time-dependent 2D barred galaxy model



Time-dependent 3D barred galaxy model

Interplay between chaotic and regular motion



Chaos diagnostics based on Lagrangian descriptors (LDs)

Lagrangian descriptors (LDs)

The computation of LDs is based on the accumulation of some positive scalar value along the path of individual orbits.

Consider an N dimensional continuous time dynamical system

$$\dot{\mathbf{x}} = \frac{d\mathbf{x}(t)}{dt} = \mathbf{f}(\mathbf{x}, t)$$

The Arclength Definition [Madrid & Mancho, Chaos (2009) – Mendoza & Mancho, PRL (2010) – Mancho et al., Commun. Nonlin. Sci. Num. Simul. (2013)].

Forward time LD:

$$\text{LD}^f(\mathbf{x}, \tau) = \int_0^\tau \|\dot{\mathbf{x}}(t)\| dt$$

Backward time LD:

$$\text{LD}^b(\mathbf{x}, \tau) = \int_{-\tau}^0 \|\dot{\mathbf{x}}(t)\| dt$$

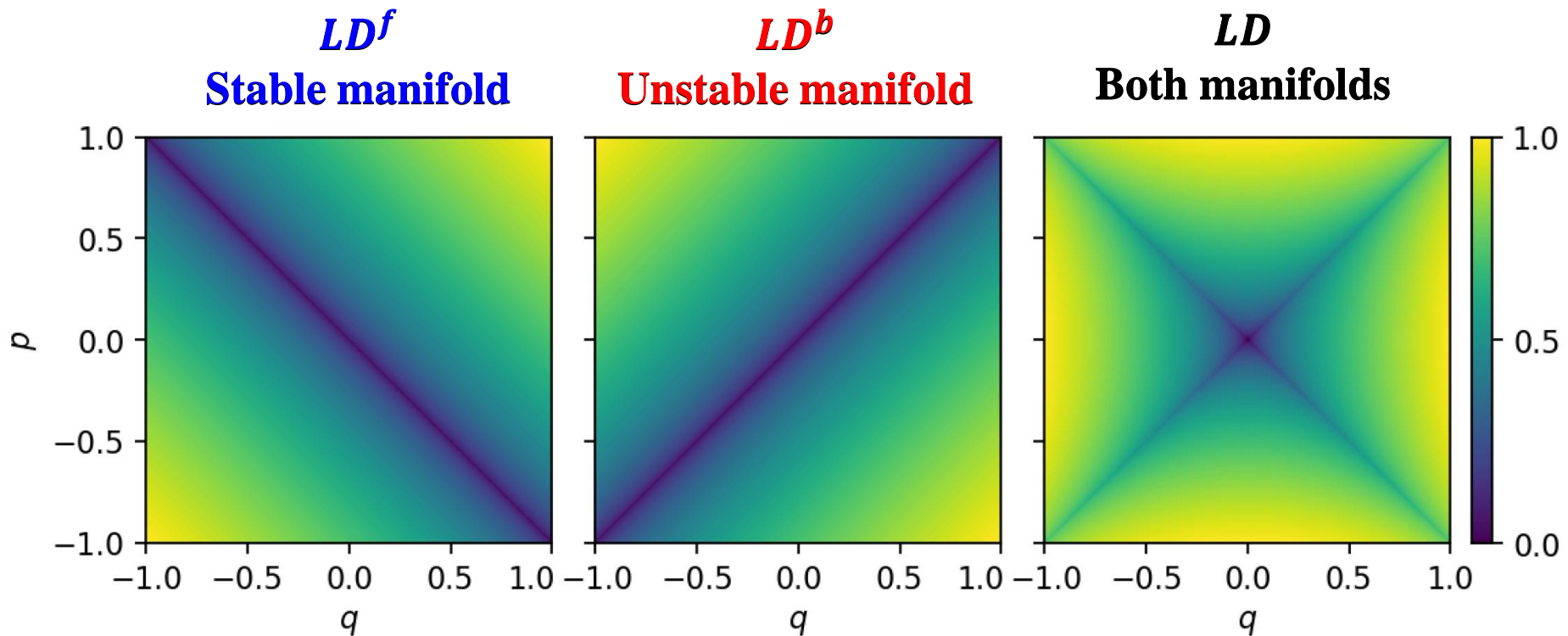
Combined LD:

$$\text{LD}(\mathbf{x}, \tau) = \text{LD}^b(\mathbf{x}, \tau) + \text{LD}^f(\mathbf{x}, \tau)$$

LDs: 1 degree of freedom (dof) Hamiltonian

$$H(q, p) = \frac{1}{2} (p^2 - q^2)$$

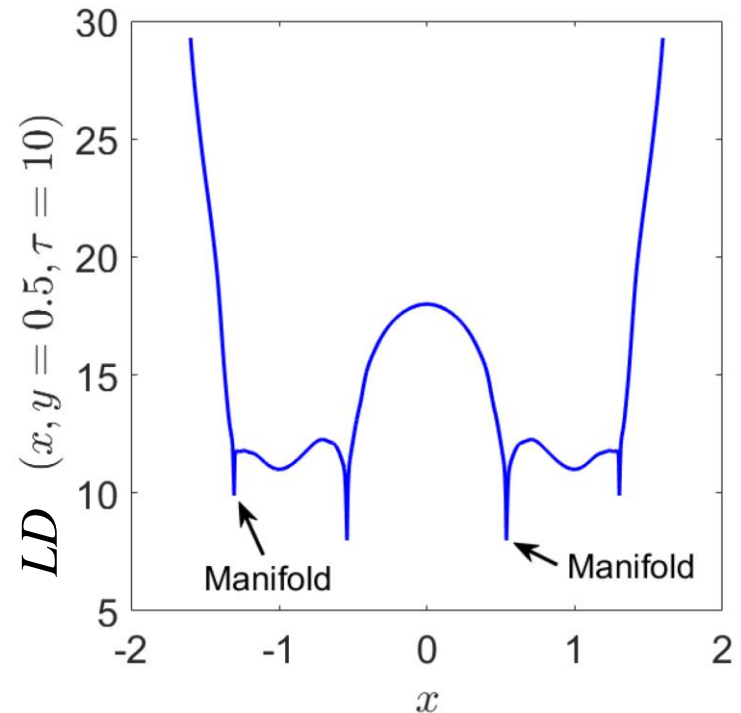
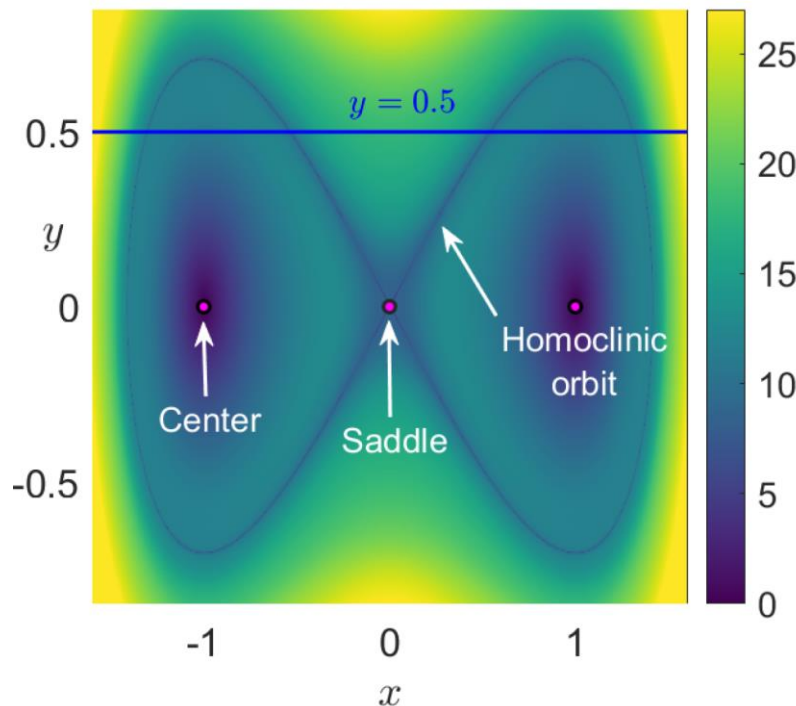
The system has a hyperbolic fixed point at the origin. The LDs can be used to display the stable and unstable manifolds of this point.



LDs: 1 dof Duffing Oscillator

$$H(x, y) = \frac{1}{2}y^2 + \frac{1}{4}x^4 - \frac{1}{2}x^2$$

The system has three equilibrium points: a saddle located at the origin and two diametrically opposed centers at the points $(\pm 1, 0)$.



From Agaoglou et al. 'Lagrangian descriptors: Discovery and quantification of phase space structure and transport', 2020, <https://doi.org/10.5281/zenodo.3958985>

The **location of the stable and unstable manifolds** can be extracted from the ridges of the **gradient field of the LDs** since they are located at points where the forward and the backward components of the LD are non-differentiable.

Lagrangian descriptors (LDs)

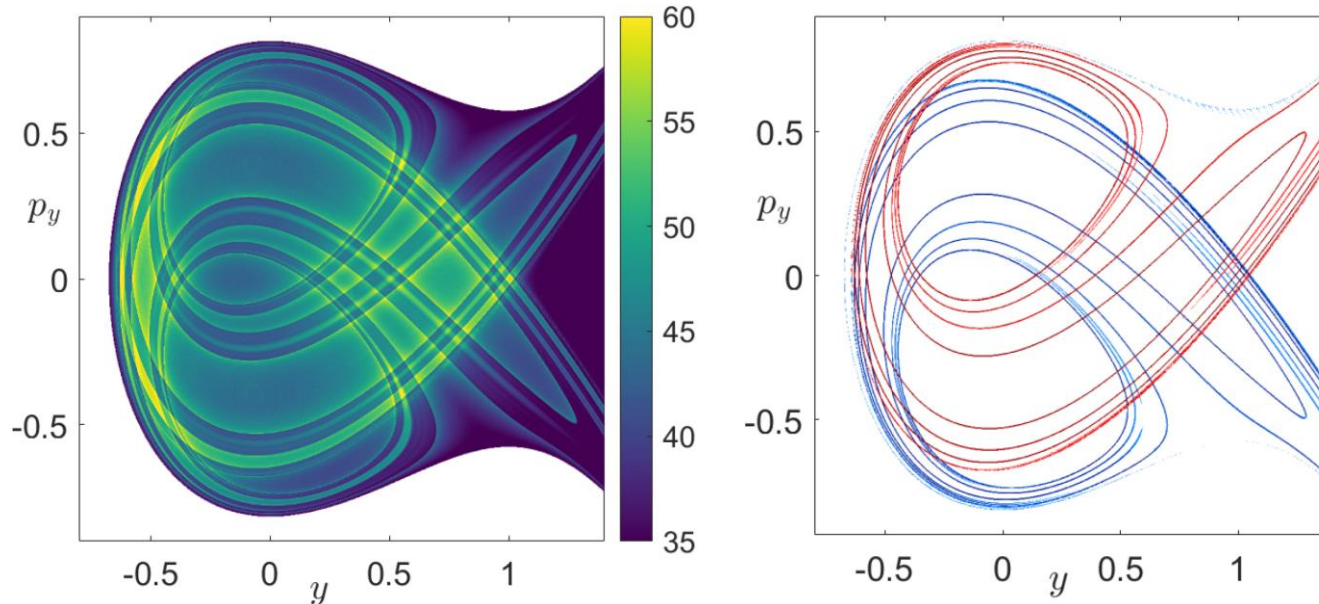
The ‘p-norm’ Definition [Lopesino et al., Commun. Nonlin. Sci. Num. Simul. (2015) – Lopesino et al., Int. J. Bifurc. Chaos (2017)].

Combined LD (usually $p=1/2$):

$$LD(\mathbf{x}, \tau) = \int_{-\tau}^{\tau} \left(\sum_{i=1}^N |f_i(\mathbf{x}, t)|^p \right) dt$$

Hénon-Heiles system: $H = \frac{1}{2} (p_x^2 + p_y^2) + \frac{1}{2} (x^2 + y^2) + x^2 y - \frac{1}{3} y^3$

Stable and unstable manifolds for $H=1/3, \tau=10$.



Using LDs to quantify chaos

We consider orbits on a finite grid of an $n(\geq 1)$ -dimensional subspace of the $N(\geq n)$ -dimensional phase space of a dynamical system and their LDs.

Any non-boundary point \mathbf{x} in this subspace has $2n$ nearest neighbors

$$\mathbf{y}_i^\pm = \mathbf{x} \pm \sigma^{(i)} \mathbf{e}^{(i)}, \quad i = 1, 2, \dots, n,$$

where $\mathbf{e}^{(i)}$ is the i th usual basis vector in \mathbb{R}^n and $\sigma^{(i)}$ is the distance between successive grid points in this direction.

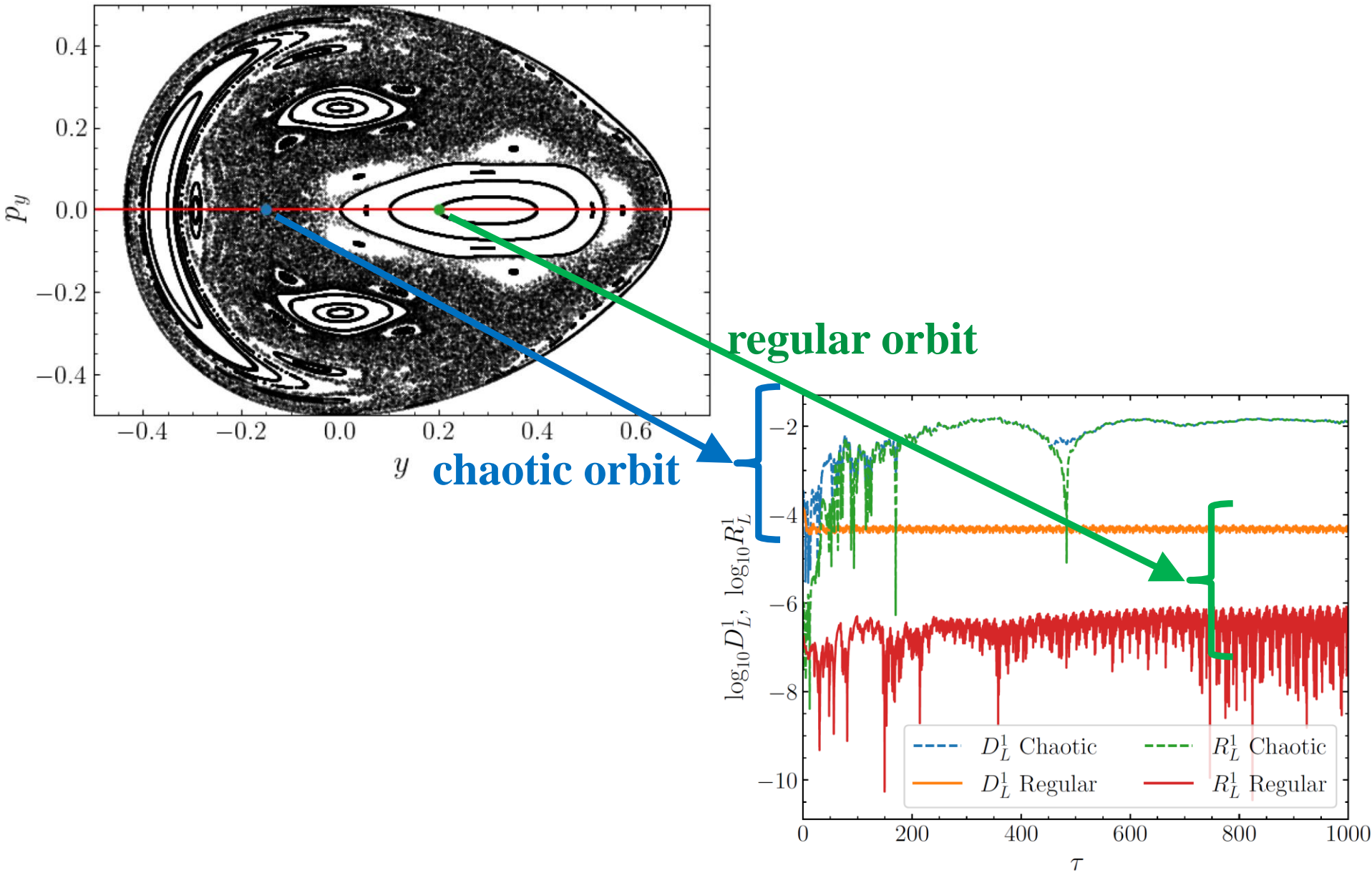
The **difference** D_L^n of neighboring orbits' LDs:

$$D_L^n(\mathbf{x}) = \frac{1}{2n} \sum_{i=1}^n \frac{|\text{LD}^f(\mathbf{x}) - \text{LD}^f(\mathbf{y}_i^+)| + |\text{LD}^f(\mathbf{x}) - \text{LD}^f(\mathbf{y}_i^-)|}{\text{LD}^f(\mathbf{x})}.$$

The **ratio** R_L^n of neighboring orbits' LDs:

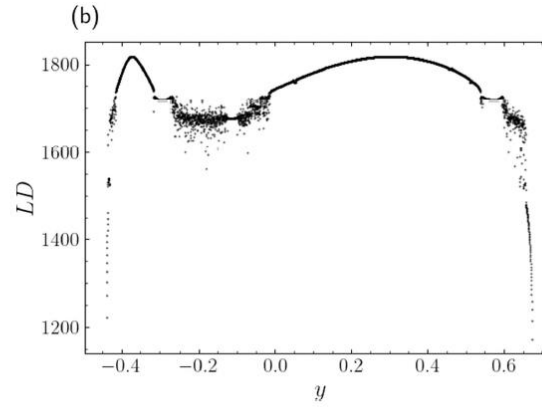
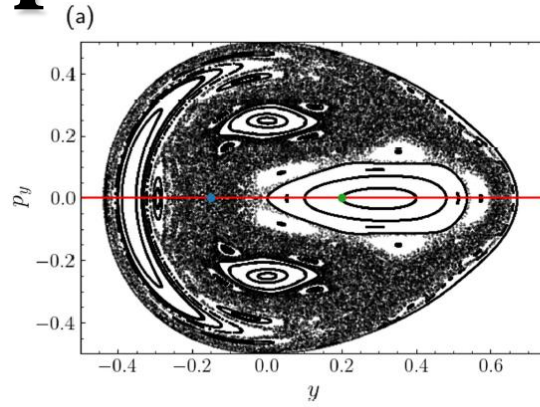
$$R_L^n(\mathbf{x}) = \left| 1 - \frac{1}{2n} \sum_{i=1}^n \frac{\text{LD}^f(\mathbf{y}_i^+) + \text{LD}^f(\mathbf{y}_i^-)}{\text{LD}^f(\mathbf{x})} \right|.$$

Application: Hénon-Heiles system



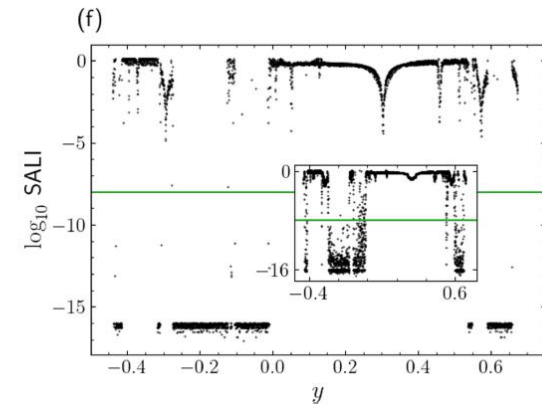
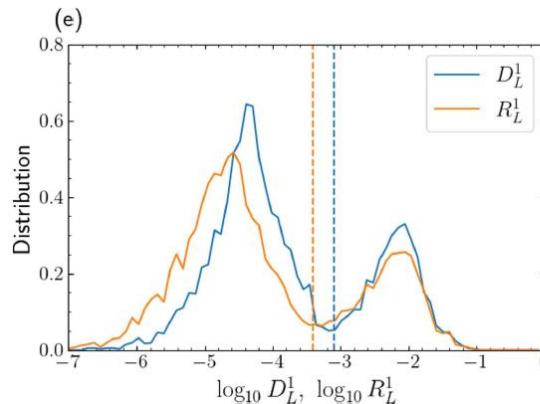
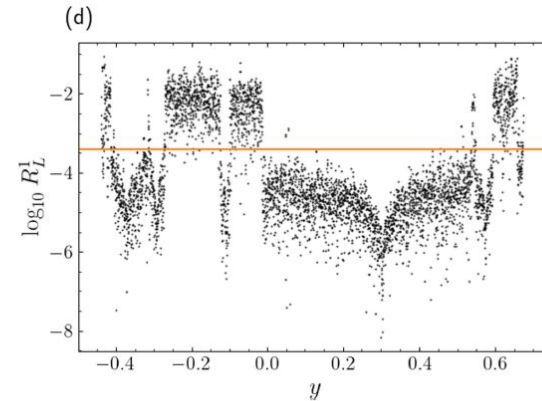
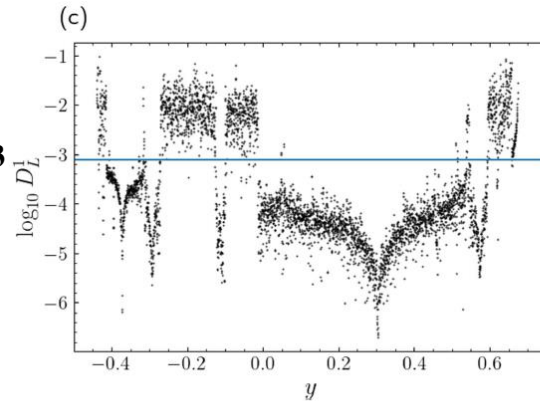
Application: Hénon-Heiles system

$H=1/8$



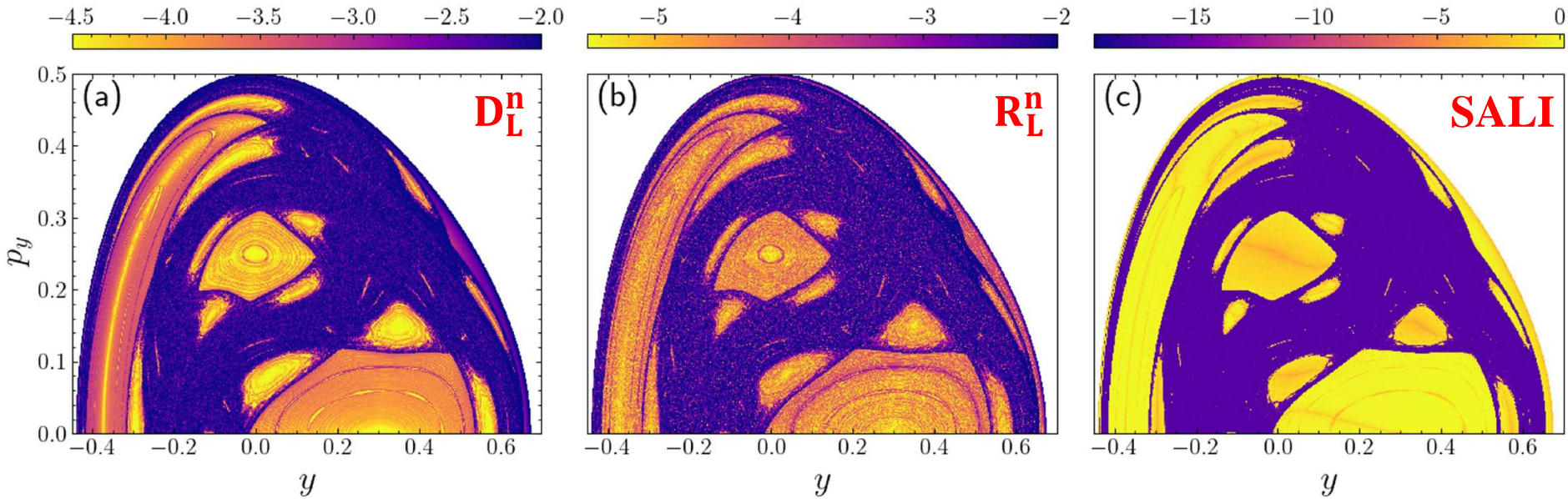
Variation of LDs with regard to initial conditions.
regular regions: smooth
chaotic regions: erratic
[also see Montes et al., Commun. Nonlin. Sci. Num. Simul. (2021)]

LDs for $\tau=10^3$

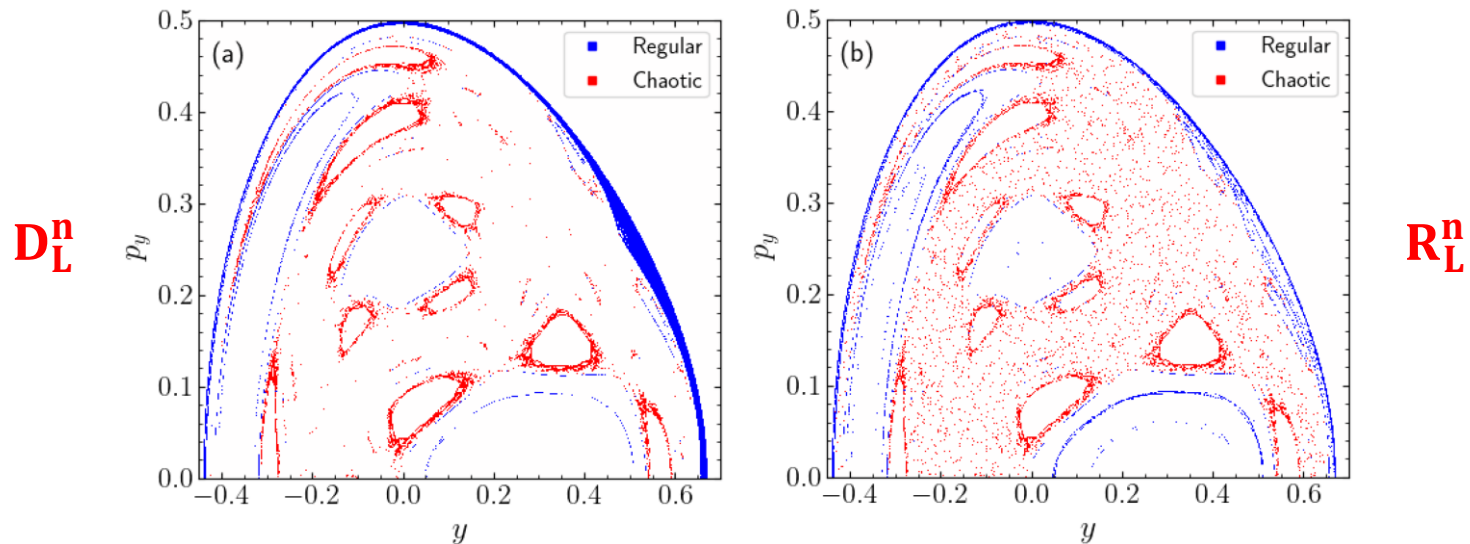


SALI for $\tau=10^6$
(inset $\tau=10^3$)

Application: Hénon-Heiles system



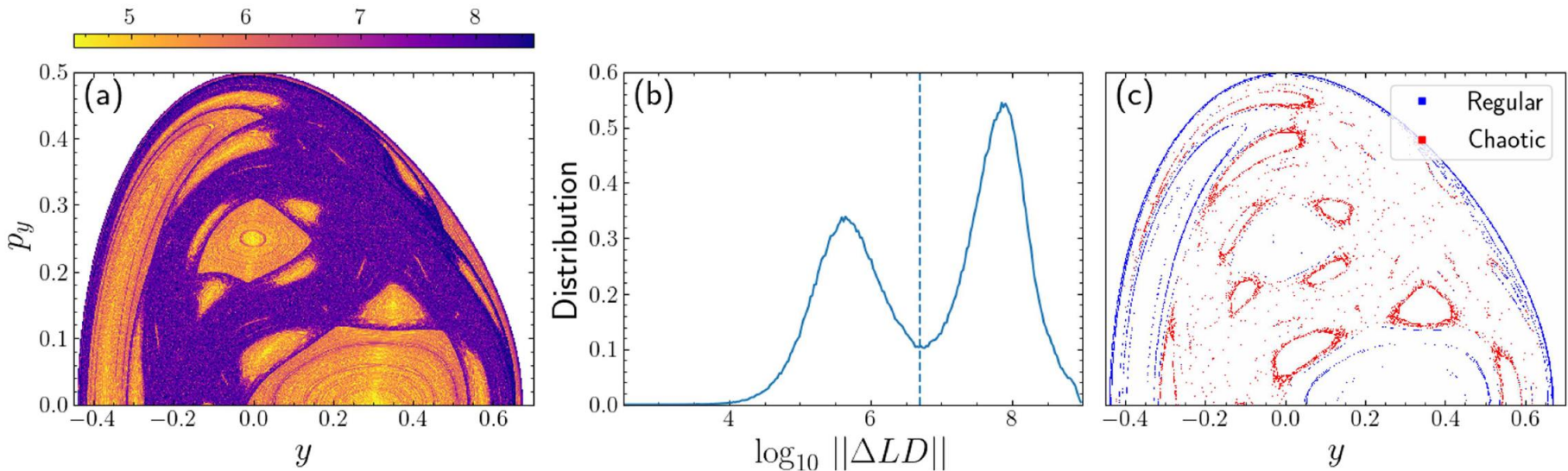
Misclassified orbits (< 10%)



Application: Hénon-Heiles system

A quantity related to **the second derivative of the LDs** was introduced in Daquin et al., Physica D (2022) and was used in Hillebrand et al., Chaos (2022) and Zimper et al., Physica D (2023):

$$\|\Delta LD\|(\mathbf{x}) = \left| \frac{LD^f(\mathbf{y}_i^+) - 2LD^f(\mathbf{x}) + LD^f(\mathbf{y}_i^-)}{\sigma^2} \right|.$$



Summary I

- We discussed methods of chaos detection based on
 - ✓ the visualization of orbits
 - ✓ the numerical analysis of orbits
 - ✓ the evolution of deviation vectors (variational equations – tangent map)
- The Smaller (SALI) and the Generalized (GALI) ALignment Index methods are **fast, efficient and easy to compute chaos indicator**.
- Behaviour of the Generalized ALignment Index of order k ($GALI_k$):
 - ✓ **Chaotic motion: it tends exponentially to zero**
 - ✓ **Regular motion: it fluctuates around non-zero values (or goes to zero following power-laws)**
- $GALI_k$ indices :
 - ✓ **can distinguish rapidly and with certainty between regular and chaotic motion**
 - ✓ **can be used to characterize individual orbits as well as "chart" chaotic and regular domains in phase space**
 - ✓ **can identify regular motion on low-dimensional tori**
 - ✓ **are perfectly suited for studying the global dynamics of multidimensional systems, as well as of time-dependent models**

Summary II

- We introduced and successfully implemented computationally efficient ways to effectively identify chaos in conservative dynamical systems from the values of LDs at neighboring initial conditions.
- From the distributions of the indices' values we determine appropriate **threshold values**, which allow the characterization of orbits as regular or chaotic.
- Both indices **faced problems** in correctly revealing the nature of some orbits mainly **at the borders of stability islands**.
- Both indices show **overall very good performance**, as their classifications are in accordance with the ones obtained by the SALI at a level of at least **90% agreement**.
- **Advantages:**
 - ✓ **Easy to compute** (actually only the forward LDs are needed).
 - ✓ **No need to know and to integrate the variational equations.**
- These methods has also been successfully applied to **2D and 4D symplectic maps** [Hillebrand et al., Chaos (2022) – Zimper et al., Physica D (2023)]

Main References I

- **The color and rotation (CR) method**
 - ✓ Patsis & Zachilas (1994) *Int. J. Bif. Chaos*, 4, 1399
 - ✓ Katsanikas & Patsis (2011) *Int. J. Bif. Chaos*, 21, 467
 - ✓ Katsanikas, Patsis & Contopoulos (2011) *Int. J. Bif. Chaos*, 21, 2321
- **the 3D phase space slices (3PSS) technique**
 - ✓ Richter, Lange, Backer & Ketzmerick (2014), *Phys. Rev. E* 89, 022902
 - ✓ Lange, Richter, Onken, Backer & Ketzmerick (2014), *Chaos* 24, 024409
 - ✓ Onken, Lange, Ketzmerick & Backer (2016), *Chaos* 26, 063124
- **Frequency Analysis**
 - ✓ Laskar (1990) *Icarus*, 88, 266
 - ✓ Laskar, Froeschle & Celletti (1992) *Physica D*, 56, 253
 - ✓ Laskar (1993) *Physica D*, 67, 257
 - ✓ Bartolini, Bazzani, Giovannozzi, Scandale & Todesco (1996) *Part. Accel.* 52, 147
 - ✓ Laskar (1999) in *Hamiltonian systems with three or more degrees of freedom* (ed. Simo / Plenum Press) p 134
- **Lyapunov exponents**
 - ✓ Oseledec (1968) *Trans. Moscow Math. Soc.*, 19, 197
 - ✓ Benettin, Galgani, Giorgilli & Strelcyn (1980) *Meccanica*, March, 9
 - ✓ Benettin, Galgani, Giorgilli & Strelcyn (1980) *Meccanica*, March, 21
 - ✓ Wolf, Swift, Swinney & Vastano (1985) *Physica D*, 16, 285
 - ✓ S. (2010) *Lect. Notes Phys.*, 790, 63

Main References II

- **0-1 test**
 - ✓ Gottwald & Melbourne (2004) Proc. R. Soc. A, 460, 603
 - ✓ Gottwald & Melbourne (2005) Physica D, 212, 100
 - ✓ Gottwald & Melbourne (2009) SIAM J. Appl. Dyn., 8, 129
 - ✓ Gottwald & Melbourne (2016) Lect. Notes Phys., 915, 221
- **FLI – OFLI – OFLI2**
 - ✓ Froeschle, Lega & Gonczi (1997) Celest. Mech. Dyn. Astron., 67, 41
 - ✓ Guzzo, Lega & Froeschle (2002) Physica D, 163, 1
 - ✓ Fouchard, Lega, Froeschle & Froeschle (2002) Celest. Mech. Dyn. Astron., 83, 205
 - ✓ Barrio (2005) Chaos Sol. Fract., 25, 71
 - ✓ Barrio (2006) Int. J. Bif. Chaos, 16, 2777
 - ✓ Lega, Guzzo & Froeschle (2016) Lect. Notes Phys., 915, 35
 - ✓ Barrio (2016) Lect. Notes Phys., 915, 55
- **MEGNO**
 - ✓ Cincotta & Simo (2000) Astron. Astroph. Suppl. Ser., 147, 205
 - ✓ Cincotta, Giordano & Simo (2003) Physica D, 182, 151
 - ✓ Cincotta, & Giordano (2016) Lect. Notes Phys., 915, 93
- **RLI**
 - ✓ Sandor, Erdi & Efthymiopoulos (2000) Celest. Mech. Dyn. Astron., 78, 113
 - ✓ Sandor, Erdi, Szell & Funk (2004) Celest. Mech. Dyn. Astron., 90 127
 - ✓ Sandor & Maffione (2016) Lect. Notes Phys., 915, 183

Main References III

- **SALI**

- ✓ S. (2001) *J. Phys. A*, 34, 10029
- ✓ S., Antonopoulos, Bountis & Vrahatis (2003) *Prog. Theor. Phys. Supp.*, 150, 439
- ✓ S., Antonopoulos, Bountis & Vrahatis (2004) *J. Phys. A*, 37, 6269
- ✓ Bountis & S. (2006) *Nucl. Inst Meth. Phys Res. A*, 561, 173
- ✓ Boreaux, Carletti, S. & Vittot (2012) *Com. Nonlin. Sci. Num. Sim.*, 17, 1725
- ✓ Boreaux, Carletti, S., Papaphilippou & Vittot (2012) *Int. J. Bif. Chaos*, 22, 1250219

- **GALI**

- ✓ S., Bountis & Antonopoulos (2007) *Physica D*, 231, 30
- ✓ S., Bountis & Antonopoulos (2008) *Eur. Phys. J. Sp. Top.*, 165, 5
- ✓ Gerlach, Eggl & S. (2012) *Int. J. Bif. Chaos*, 22, 1250216
- ✓ Manos, S. & Antonopoulos (2012) *Int. J. Bif. Chaos*, 22, 1250218
- ✓ Manos, Bountis & S. (2013) *J. Phys. A*, 46, 254017

- **Reviews on SALI and GALI**

- ✓ Bountis & S. (2012) 'Complex Hamiltonian Dynamics', Chapter 5, Springer Series in Synergetics
- ✓ S. & Manos (2016) *Lect. Notes Phys.*, 915, 129

Main References IV

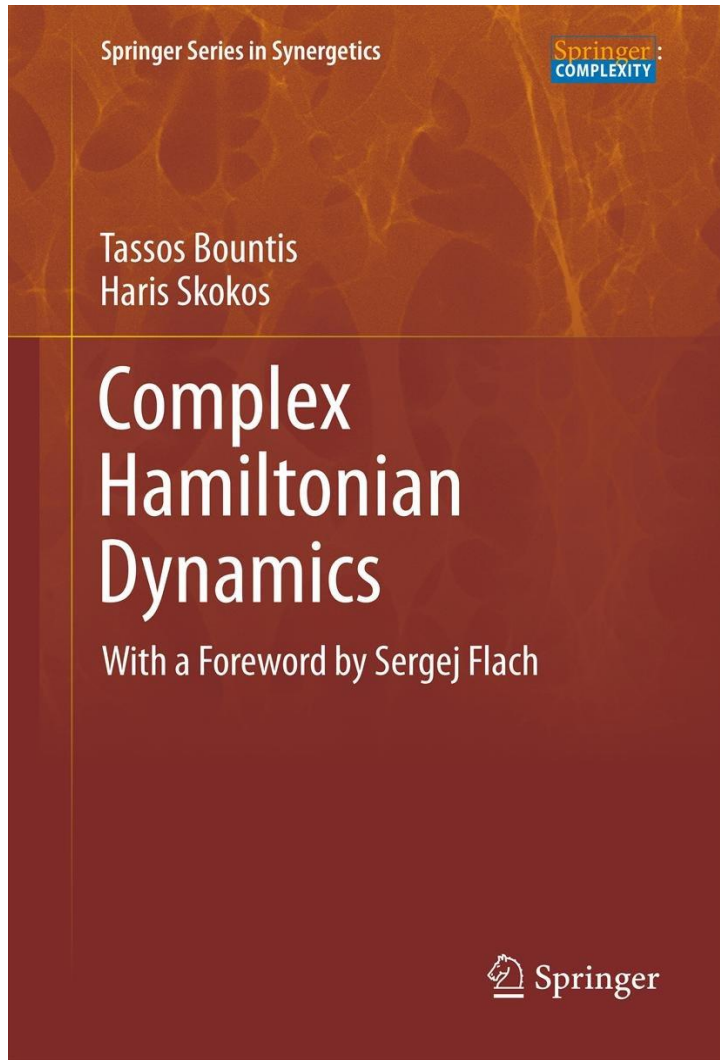
- **Lagrangian descriptors (LDs)**

- ✓ Madrid & Mancho (2009) *Chaos*, 19, 013111
- ✓ Mendoza & Mancho (2010) *Phys. Rev. Lett.*, 105, 038501
- ✓ Mancho, Wiggins, Curbelo & Mendoza (2013) *Commun. Nonlin. Sci. Num. Simul.*, 18, 3530
- ✓ Lopesino, Balibrea, Wiggins & Mancho (2015) *Commun. Nonlin. Sci. Num. Simul.*, 27, 40
- ✓ Lopesino, Balibrea-Iniesta, García-Garrido, Wiggins & Mancho, (2017) *Int. J. Bifurc. Chaos*, 27, 1730001
- ✓ Agaoglou, Aguilar-Sanjuan, García-Garrido, González-Montoya, Katsanikas, Krajnák, Naik & Wiggins (2020) ‘Lagrangian descriptors: Discovery and quantification of phase space structure and transport’, <https://doi.org/10.5281/zenodo.3958985>
- ✓ Montes, Revuelta & Borondo (2021) *Commun. Nonlin. Sci. Num. Simul.*, 102, 105860
- ✓ Daquin, Pédenon-Orlanducci, Agaoglou, García-Sánchez & Mancho (2022) *Physica D*, 442, 133520

- **Chaos diagnostics based on LDs**

- ✓ Hillebrand, Zimper, Ngapasare, Katsanikas, Wiggins & S. (2022) *Chaos*, 32, 123122
- ✓ Zimper, Ngapasare, Hillebrand, Katsanikas, Wiggins & S. (2023) *Physica D*, 453, 133833

A ...shameless promotion



Contents

1. Introduction
2. Hamiltonian Systems of Few Degrees of Freedom
3. Local and Global Stability of Motion
4. Normal Modes, Symmetries and Stability
5. Efficient Indicators of Ordered and Chaotic Motion
6. FPU Recurrences and the Transition from Weak to Strong Chaos
7. Localization and Diffusion in Nonlinear One-Dimensional Lattices
8. The Statistical Mechanics of Quasi-stationary States
9. Conclusions, Open Problems and Future Outlook

2012, Springer Series in Synergetics

Another ...shameless promotion

Contents

Lecture Notes in Physics 915

Charalampos (Haris) Skokos
Georg A. Gottwald
Jacques Laskar *Editors*

Chaos Detection and Predictability

 Springer

1. **Parlitz: Estimating Lyapunov Exponents from Time Series**
2. **Lega, Guzzo, Froeschlé: Theory and Applications of the Fast Lyapunov Indicator (FLI) Method**
3. **Barrio: Theory and Applications of the Orthogonal Fast Lyapunov Indicator (OFLI and OFLI2) Methods**
4. **Cincotta, Giordano: Theory and Applications of the Mean Exponential Growth Factor of Nearby Orbits (MEGNO) Method**
5. **S., Manos: The Smaller (SALI) and the Generalized (GALI) Alignment Indices: Efficient Methods of Chaos Detection**
6. **Sándor, Maffione: The Relative Lyapunov Indicators: Theory and Application to Dynamical Astronomy**
7. **Gottwald, Melbourne: The 0-1 Test for Chaos: A Review**
8. **Siegert, Kantz: Prediction of Complex Dynamics: Who Cares About Chaos?**